AD-A178 084 NAVY PRODUCT IMPROVEMENT PROGRAM FOR TURBOMACH T-62T APU'S-CORROSION RESI (U) SUNDSTRAND TURBOMACH SAN DIEGO CA W A ROBERTSON 12 MAY 86 ERR-0632 1/1

UNCLASSIFIED N00019-80-G-0603 F/G 11/6 NL

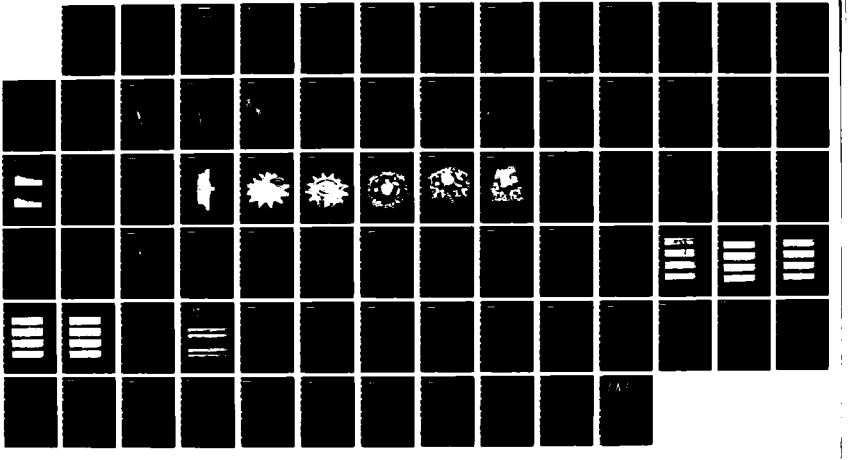

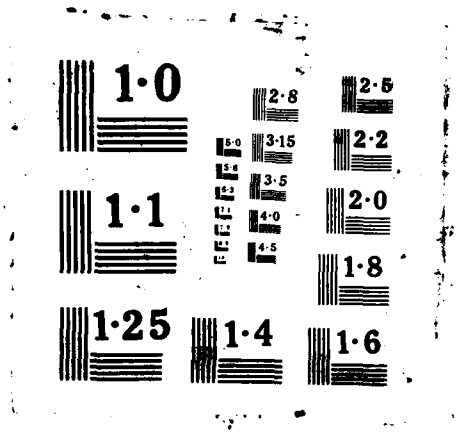
1·0
1·1
1·25
2·8
3·15
3·5
4·0
4·5
5·0
1·4
2·5
2·2
2·0
1·8
1·6

AD-A178 084

Report ERR 0632

NAVY PRODUCT IMPROVEMENT PROGRAM FOR TURBOMACH T-62T APU'S - CORROSION RESISTANT TURBINE WHEEL/IMPROVED BEARING AND LUBRICATION SYSTEM

DTIC
ELECTE
MAR 1 9 1987
D

Wade A. Robertson
Sundstrand Turbomach
4400 Ruffin Road
P.O. Box 85757
San Diego, CA 92138-5757

12 May 1986

Final Report for Period 19 January 1983 - 12 April 1986

APPROVED FOR PUBLIC RELEASE:
DISTRIBUTION UNLIMITED

Prepared for

DEPARTMENT OF THE NAVY
Naval Air Systems Command
AIR-536
Washington, D.C. 20361

DCASMA-San Diego
4297 Pacific Highway
San Diego, CA 92110
Admin: GSCB-74/[redacted]

DTIC FILE COPY

Turbomach
division of Sundstrand Corporation
SUNDSTRAND
4400 RUFFIN ROAD, P.O. BOX 85757 • SAN DIEGO, CALIFORNIA 92138-5757

FSCM 55820

REPORT

NAVY PRODUCT IMPROVEMENT PROGRAM FOR TURBOMACH T-62T AUXILIARY POWER UNITS

CORROSION RESISTANT TURBINE WHEEL/IMPROVED BEARING AND LUBRICATION SYSTEM

DATA CONTROL LEVEL

RELEASE STAMP

DOCUMENT NO.: ERR 0632 ISSUED: (DATE AND ERL NO.) 12 May 1986

REVISION: (LETTER, DATE AND ERL NO.)

Customer Ref:
BOA N00019-80-G-0603, VH03

Solar Ref:
S.O. 4-00318

PREPARED BY:

W. A. Robertson
Associate Engineer

APPROVED BY:

C. S. Martineau
Senior Project Engineer

R. W. Smith
Senior Project Engineer

Turbomach
division of Sundstrand Corporation
4400 RUFFIN ROAD, P.O. BOX 85757 • SAN DIEGO, CALIFORNIA 92138-5757
FSCM 55820

ERR 0632
ISSUED: 12 May 1986

CONTENTS

Accesion For
NTIS CRA&I ☑
DTIC TAB ☐
Unannounced ☐
Justification
By
Distribution /
Availability Codes
Dist | Avail and / or Special
A-1

INSPECTED 4

LIST OF FIGURES

LIST OF TABLES

LIST OF PHOTOGRAPHS

APPENDICES

Turbomach
division of Sundstrand Corporation
4400 RUFFIN ROAD, P.O. BOX 85757 • SAN DIEGO, CALIFORNIA 92138-5757
FSCM 55820

ERR 0632
ISSUED: 12 May 1986

I. CORROSION RESISTANT TURBINE WHEEL PROGRAM

1.0 INTRODUCTION

Sundstrand Turbomach has received Contract N00019-8-G-0603 from the United States Department of the Navy, Naval Air Systems Command, Washington, D.C., for the purpose of conducting a product improvement program for Turbomach T-62T auxiliary power units. The program consists of two areas of investigation:

1) Corrosion Resistant Turbine Wheel
2) Improved Bearing and Lubrication

Section I of this report discusses the Corrosion Resistant Turbine Wheel investigation and satisfies the final requirement of the program. This report represents the completion of the obligations as defined in the Statement of Work.

1.1 PROGRAM STATUS

The following table details the status of obligations defined in the Statement of Work.

Statement of Work - Task Status

I. Corrosion Resistant Turbine Wheel

Task	Status
Perform Turbine Wheel Analysis and Prepare Turbine Life Predictions	Complete
Design Turbine Wheel	Complete
Prepare Material Specification	Complete
Manufacture Tooling	Not Required

Statement of Work - Task Status (Continued)

I. Corrosion Resistant Turbine Wheel

Task	Status
Procure Castings	Complete
Perform Casting Qualification	Complete
Conduct a Burst Test to Establish Rim Failure Mode	Complete
Perform a Holographic Analysis	Complete
Prepare Comparative Sulfidation Resistance Predictions	Complete
Perform Project Management	Complete
Prepare Final Report	Complete

1.2 BACKGROUND

Titan T-27 and T-40-1 gas turbine engines have used IN-713 LC turbine wheels for many years without serious hot corrosion problems. For extended operation in marine environments, however, the well-known susceptibility of Alloy 713 to hot corrosion (sulfidation) could lead to deterioration of airfoil surfaces resulting eventually in loss of engine performance, or even engine failure.

Corrosion protection could be enhanced by protective coatings; however, with a base material so poor in hot corrosion resistance as Alloy 713, the reliability of a 713 turbine wheel would be suspect. Also, the degradation of mechanical properties accompanying the coating process would reduce the safety margin below acceptable levels. The coatings would also be erosion sensitive. A better alternative appears to be a material change to an alloy with better hot corrosion resistance. The alloy selected was MAR-M247, a nickel-based alloy with 10 percent cobalt, 10 percent tungsten, 8.25 percent chromium, 5.5 percent aluminum, 3 percent tantalum, 1.5 percent hafnium, 1 percent titanium, and other elements. The expected improvements over IN-713 LC include improved oxidation/hot corrosion resistance, blade creep resistance, and tensile strength.

1.3 CONCLUSION

The analyses performed under the alternate material turbine wheel program indicate that the use of the MAR-M247 GX alloy will result in significant improvement in the life of the turbine wheel. Considerable advances in LCF life and stress rupture life were concluded while burst margin and high cycle fatigue analyses also showed very favorable results (Table I). Further development of heat treatment procedures is recommended prior to qualification testing.

Table I. Turbine Wheel Life Predictions

	42523 (T40-1) IN-713LC	163352 (New Design) MAR-M247 GX
Stress rupture	6,000 hours	88,000 hours
Low cycle fatigue	1,900 cycles (undercut)	12,000 (bore)
Burst margin	144 percent	159 percent

Although the test results for MAR-M247 GX appear very promising, further consideration of the alloy is dependent upon allocation of the funds necessary for further development of heat treatment procedures and qualification tests. The qualification tests would include:

- Piggyback turbine wheel qualification with compressor wheel qualification.
- Performance tests.
- Qualification test - 200 hours, 1000 starts.

As a result of the current program, three MAR-M247 GX turbine wheels are available for testing.

1.4 TURBINE WHEEL LIFE PREDICTIONS

The purpose of the alternate material turbine wheel program (S/O 4-00318) was to replace the current alloy (INCO 713LC) used in the T62-T40-1 turbine wheel (P/N 42523) with an alloy that is more resistant to hot corrosion. After surveying the promising alloys, MAR-M-247 GX was selected. In addition to a material change, it was proposed that the geometry also be updated. The combination of these changes (P/N 163352) will significantly increase the life of the turbine wheel. Analysis predicts that minimum stress rupture life will improve from 6000 hours to 88,000 hours, and low cycle fatigue life of the new design will improve from 4500 cycles to more than 12,000 cycles.

The current, or baseline, turbine wheel (P/N 42523) is characterized by the deep, as-cast surface of the backface. This design insured that any hub failure would be a low energy rim-shed. In fact, the only two hub failures to date were of this type occurring at 4500 and 5500 cycles, respectively. It is important to note that the engines that failed were equipped with a "battle switch". This device allowed the operator to override the fuel schedule and reach exhaust gas temperatures above the rated 1200°F limit. The elevated temperatures produce higher thermal stresses and can significantly reduce LCF life.

On the other hand, the proposed turbine wheel (P/N 163352) is characterized by the shallow, machined surface of its undercut. This provides two important improvements. First, a machined surface exhibits better fatigue properties than does a cast surface. Second, the more shallow backface cut reduces stress and increases life in that area. However, stress is still high enough that overspeed failure is in the relatively low-energy rim-shed mode (Section 1.7). Bore and scallop dimensions of the wheel are essentially identical to its predecessor. Furthermore, the aerodynamics of the turbine blade remain unchanged.

Turbine wheel life predictions must cover four areas: stress rupture, low cycle fatigue (LCF), burst margin, and high cycle fatigue. A turbine wheel thermal analysis was also performed to support the LCF analysis and is reported in Section 1.5. The topic of high cycle fatigue life for the proposed wheel is discussed under Blade Vibration, Section 1.6.

1.4.1 Stress (Creep) Rupture

Predicted minimum stress rupture life for the new wheel is 88,000 hours. This is in contrast to the 6000 hours predicted for the baseline wheel.

1.4.2 Low Cycle Fatigue Life

LCF life for the proposed wheel is estimated to be around 12,000 cycles and is limited by the fatigue life of the bore. Estimated LCF life for the baseline wheel was limited to 1900 cycles by the wheel's undercut. However, the service revealed life of the baseline wheel has exceeded 4000 cycles. In general, these analytic predictions represent a worst case analysis. Actual LCF life may be significantly greater than estimates indicate.

1.4.3 Burst (Overspeed) Margin

Calculations indicate that the turbine wheel can overspeed to 159 percent of nominal engine speed before failure occurs. This is based upon an average tangential stress in the wheel of 48.7 ksi and a typical ultimate tensile strength of 123.8 ksi at 1000°F. These numbers were verified by the testing described in Section 1.7 during which burst occurred at 154 percent speed. The failure mode was demcnstrated to be the relatively low energy rim-shed.

1.5 TURBINE WHEEL THERMAL ANALYSIS

A steady state and transient temperature analysis has been completed on the T-62T-40-1 turbine and compressor wheels. The scope of the analysis required the temperature distribution calculation of two turbine wheel materials, P/N's 42523 (INCO 713 LC) and 163352 (MAR-M 247 GX). However, the thermal and transport properties of the two materials are quite similar, meaning that the temperature response and steady state temperature distribution will be nearly identical. Therefore, only the steady state temperature distribution for the 42523 wheel was reported. The 163352 wheel was analyzed for both steady state and transient temperature response.

The components analyzed included the rotating components aft of the powerhead bearing centerline, that is, the turbine and compressor wheels, the tie bolt, and the shaft. The seal plate assembly was the only static part that was included.

The primary purpose of the analysis was to support the turbine wheel LCF life prediction analysis. Since the LCF analysis did not show a temperature distribution level or temperature gradient adversely affecting turbine wheel life, additional studies on schemes to correct or improve life will not be necessary.

1.6 TURBINE WHEEL BLADE VIBRATION

The current turbine wheel is characterized by the deep, as-cast surface of the backface while the proposed turbine wheel has a more shallow backface cut. This change in geometry, along with the changes in elastic modulus and density of the new material, would change the vibrational characteristics of the blade. For this reason, it became necessary to perform a vibration test and analysis in order to identify possible high cycle fatigue problems. The results of this analysis suggest that it is unlikely that there will be high cycle fatigue failure in the new turbine blade. The first natural frequency is higher than the third engine order. Minimum speed margins at the four

remaining prominent engine orders, third, fourth, eighth and sixteenth, are 15.8, -8.2, 5.4, and 4.2 percent, respectively.

The first step of the vibration analysis was holographic testing of a single turbine wheel. Results of the analysis were recorded on video tape and summarized on a data sheet. The video tape is on file at Turbomach according to the serial number of the test specimen. In this case, the wheel tested was S/N 1653-H202. After reviewing both the tape and the data sheet, the first eight natural frequencies were found. A frequency band is associated with seven of the eight frequencies. The widest band is 417 Hz and occurs around the third natural frequency. The seventh natural frequency is the exception in that all twelve blades vibrate at exactly the same frequency (21821 Hz). Such behavior usually implies that the mode is coupled to some other portion of the structure. In this case, the holographic testing of the backface showed that this seventh mode is strongly coupled to the backface and, as a result, the entire wheel vibrates at 21821 Hz.

FEM vibration results for a typical blade held at room temperature are summarized in the second column of Table II. Natural frequencies were computed for both the static and 100 percent rotational speed cases. The perspective plots of the first three modes appear in Figure 1. Although these drawings give a clear picture of blade deflections in these three cases, the deflection of the higher modes becomes more difficult to see. For this reason, as well as to help in comparing with the holograph, it is better to draw displacement contours on a 2-D blade. The first nine such plots appear in Figure 2. These shapes matched up well with the holographic data. Testing of these engines has shown that high vibrational energy was associated with the following engine orders: 3, 4, 6, 7, 8, 12, 16 and 17. Figure 3 contains the frequency spectrums for the T-62T-40-1 engine. The configuration of the engine does much to determine which engine orders will provide large excitations. For instance, the twelfth E.O. is attributed to the twelve turbine blades in the turbine wheel, the seventeenth is caused by the seventeen guide vanes in the diffuser assembly, and the eighth and sixteenth are related to the eight long and eight short blades on the compressor wheel.

The minimum speed margin for these critical engine orders was 15.8, 8.2, 38.8, 20.0, 5.4, 14.3, 4.2 and 0, respectively. With the exception of the seventeenth order margin these margins were deemed large enough to avoid high cycle failure of the turbine blade. In light of the acceptable margins at all other strong E.O.'s, no corrective action was recommended. If failure does occur due to seventeenth order interference, the blade tuning specification can be changed. However, this would almost certainly lead to smaller margins at the lower E.O.'s. At this time, the conservative approach is to postpone action that would reduce some margins until it is shown that the seventeenth E.O. presents a problem.

Table II. Summary of Stress Stiffening Effects Upon the First Eight Natural Frequencies (P/N 163352)

FINITE ELEMENT MODELING			HOLOGRAPHIC TESTING		
MODE NO. (-)	NATURAL FREQUENCY 0% SPEED/ 100% SPEED (HZ)	STIFFENING FACTOR, X (-)	MODE NO. (-)	STATIC, ROOM TEMP. NATURAL FREQUENCY (HZ)	STRESS STIFF-ENED FREQ. (HZ)
1	3846./ 4141.	2.24	1	3441.- 3554.	3768.- 3871.
2	8824./ 9127.	5.17	2	8866.- 9283.	9168.- 9571.
3	11301./ 11508.	4.48	3	9956.- 10369.	10190.- 10594.
4	17263./ 17383.	3.95	4	14792.- 14973.	14932.- 15111.
5	18816./ 19298.	17.45	5	17635.- 17760.	18148.- 18270.
6	21008./ 21068.	2.40	6	21549.- 21619.	21607.- 21677
-	- / -	3.95	7	21821.	21916.
8	26715./ 26765.	2.54	8	22808.- 22955.	22867.- 23013.

Like the seventeenth, the ninth, tenth, and fourteenth E.O.'s also interfere with natural frequencies inherent in the turbine blades. However, these E.O.'s are known to be low-energy sources and no failures are anticipated due to this cross-over. Frequency cross-over occurs when a frequency band extends above and below a certain engine order. For instance, the engine order band for the second mode at 800°F EGT was 8.68-9.07. In this case ninth order interference was possible. Furthermore, a change in EGT can also cause cross-over. For instance, when the EGT goes from 1000 to 1200°F, the engine order band drops through an engine order: 14.03-14.20 drops to 13.71-13.88. Again, blade failure is unlikely in these cases because the vibrational energy is relatively low.

The data presented here provides reason to believe that the turbine blades on P/N 163352 will not experience high cycle fatigue failure. With the exception of the seventeenth E.O., vibration interference with the high energy engine orders is avoided. If failure can be attributed to the seventeenth order interference, blade tuning will almost certainly reduce the other margins. For this reason, no action is recommended until a hardware problem arises. The next smallest speed margin in this category is the 4.2 percent margin between the fifth frequency and the sixteenth engine order. Other possible vibrational interferences are deemed unlikely because they involve relatively low energy excitations.

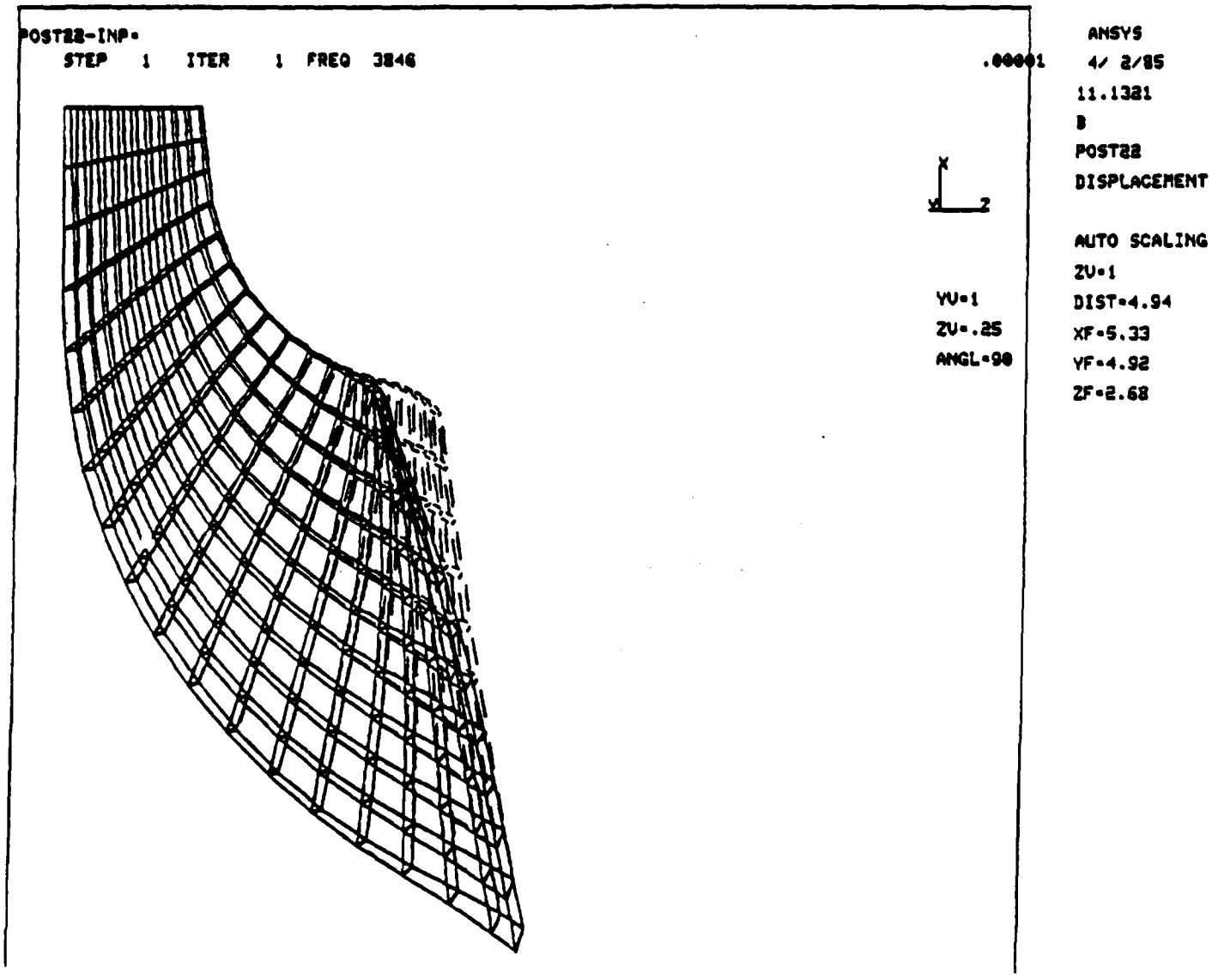

Figure 1A. Perspective Plots for First Mode (3846 Hz)
Predicted by ANSYS Modeling.

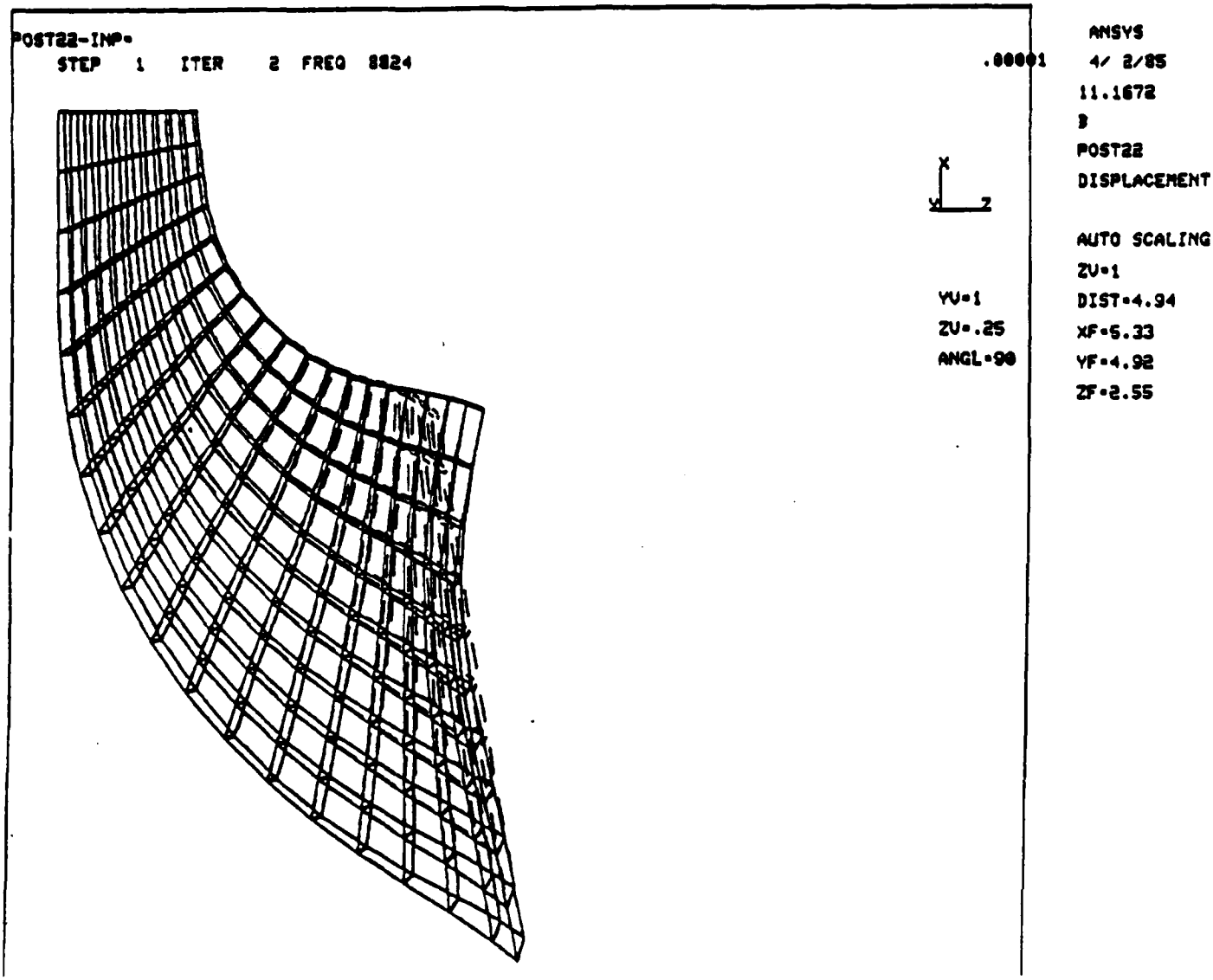

Figure 1B. Perspective Plots for Second Mode (8824 Hz) Predicted by ANSYS Modeling.

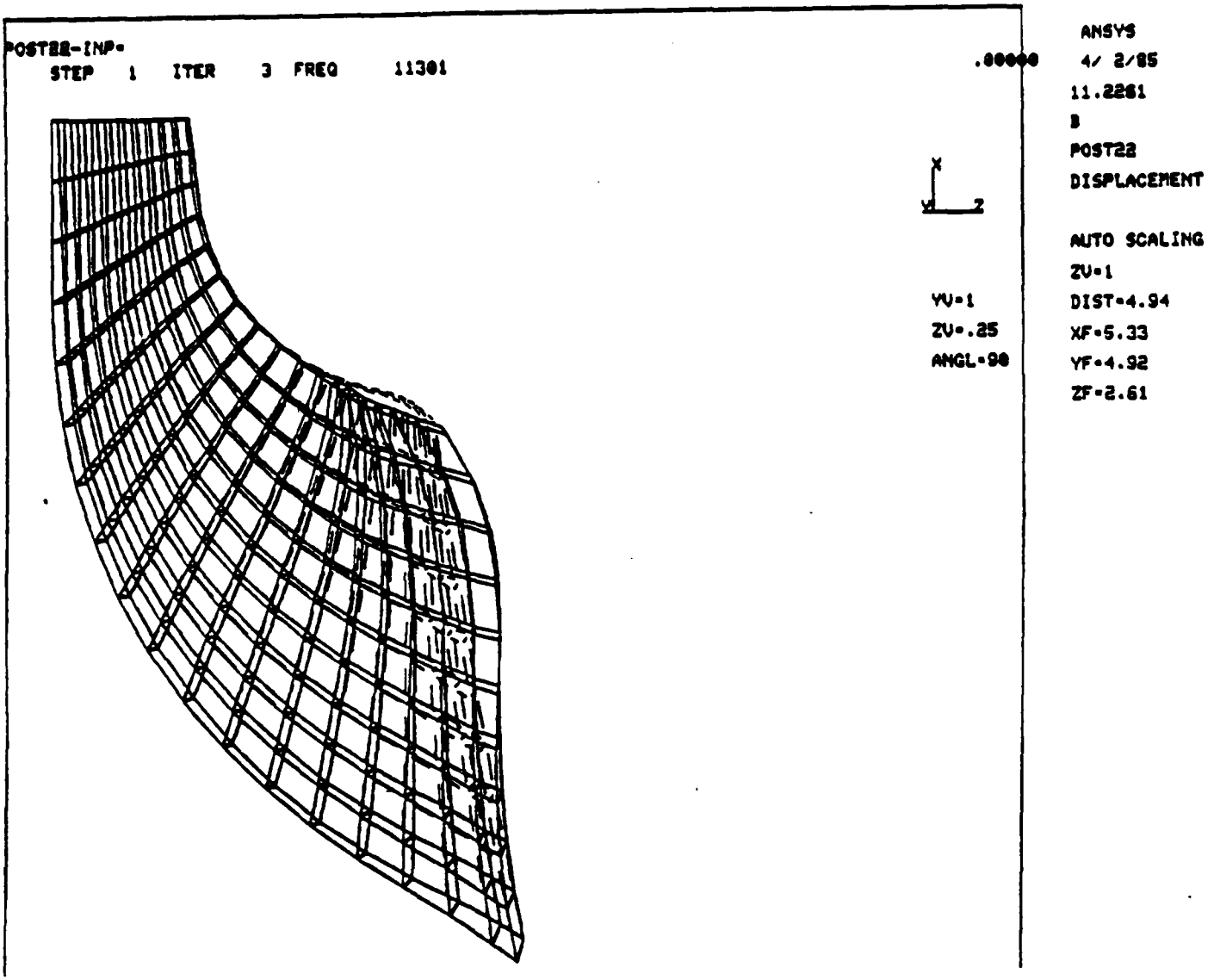

Figure 1C. Perspective Plots for Third Mode (11301 Hz)
Predicted by ANSYS Modeling

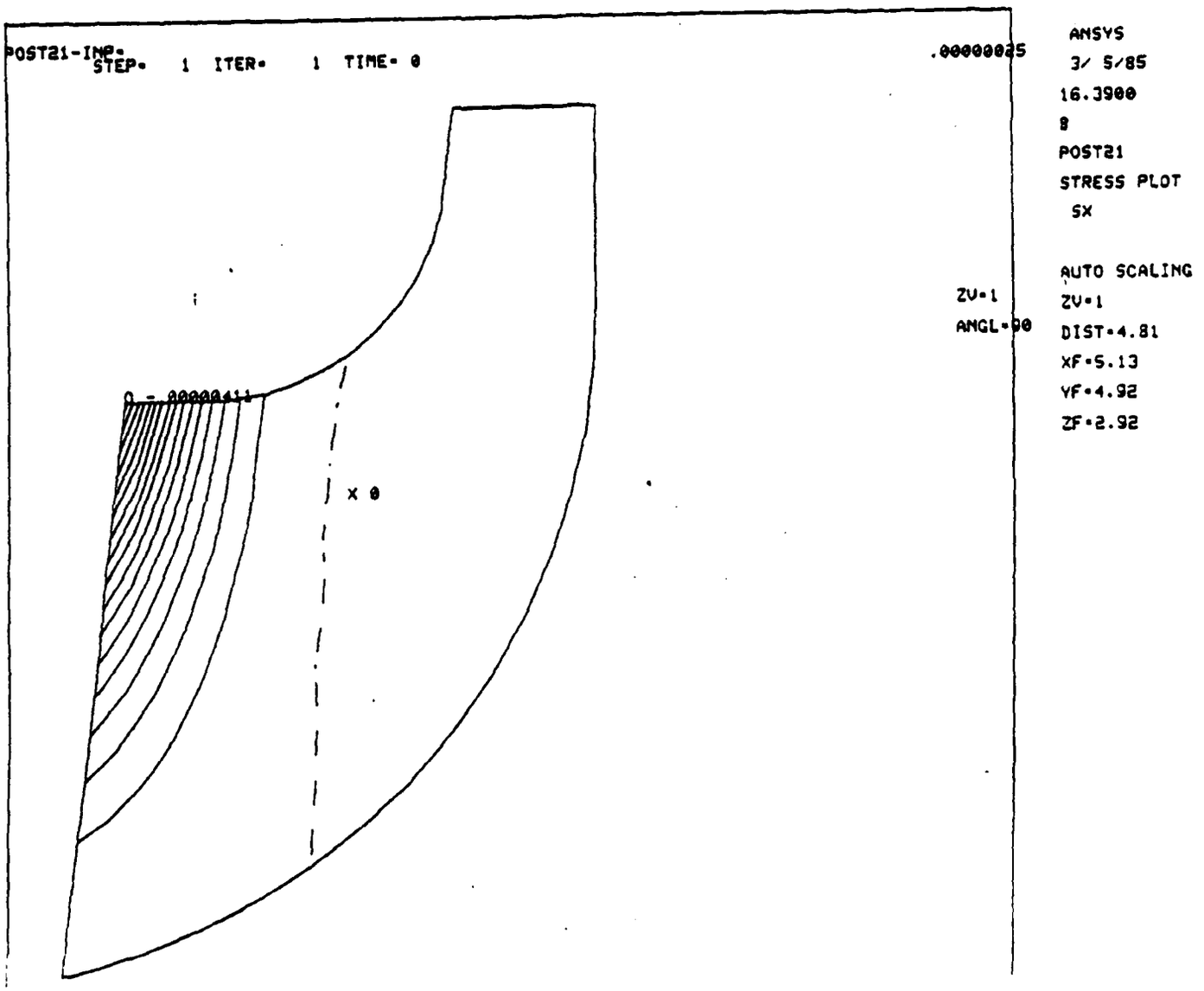

Figure 2A. Displacement Contour Plot for First Mode (3846 Hz)
Predicted by ANSYS Modeling

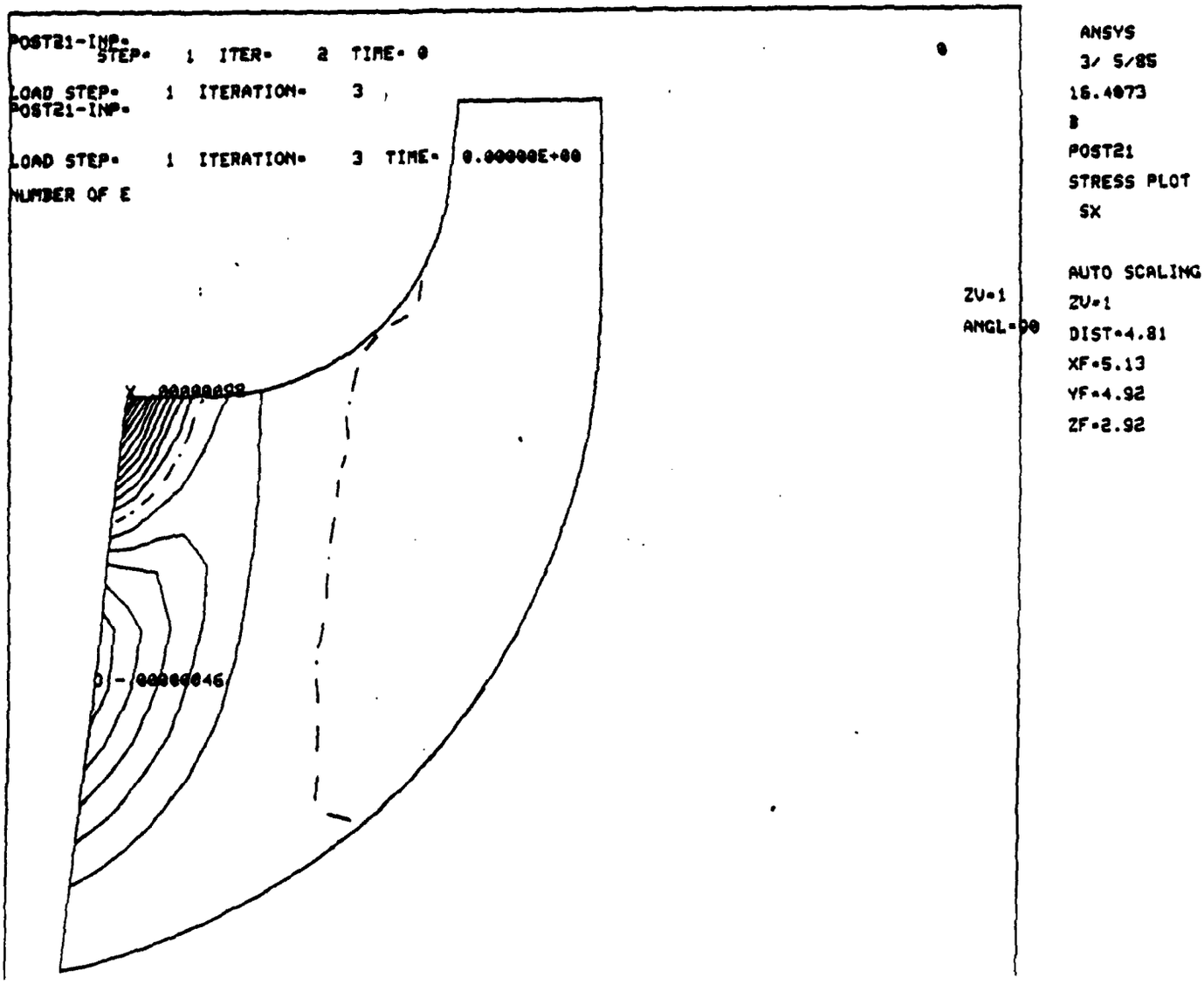

Figure 28. Displacement Contour Plot for Second Mode (8824 Hz) Predicted by ANSYS Modeling

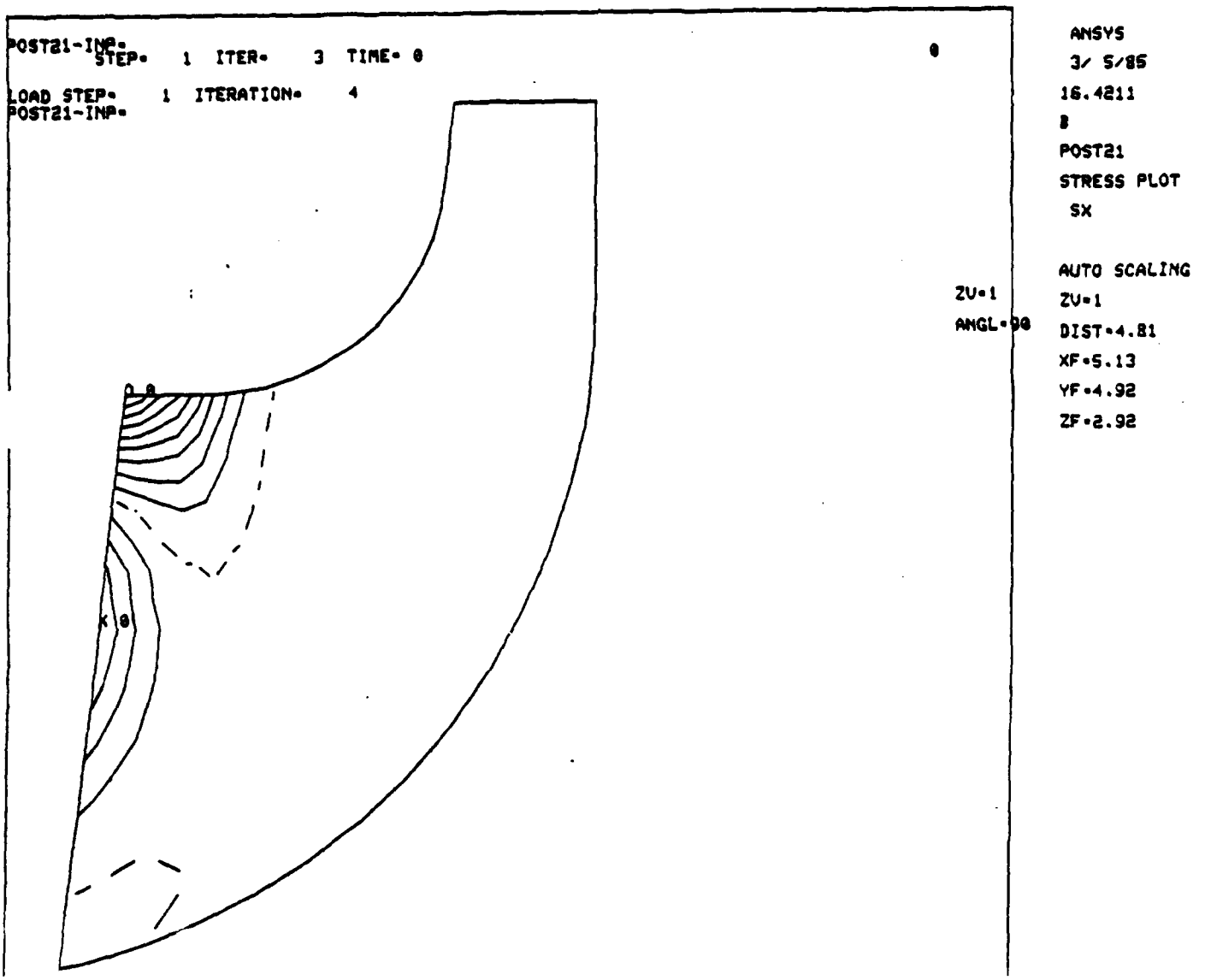

Figure 2C. Displacement Contour Plot for Third Mode (11301 Hz)
Predicted by ANSYS Modeling

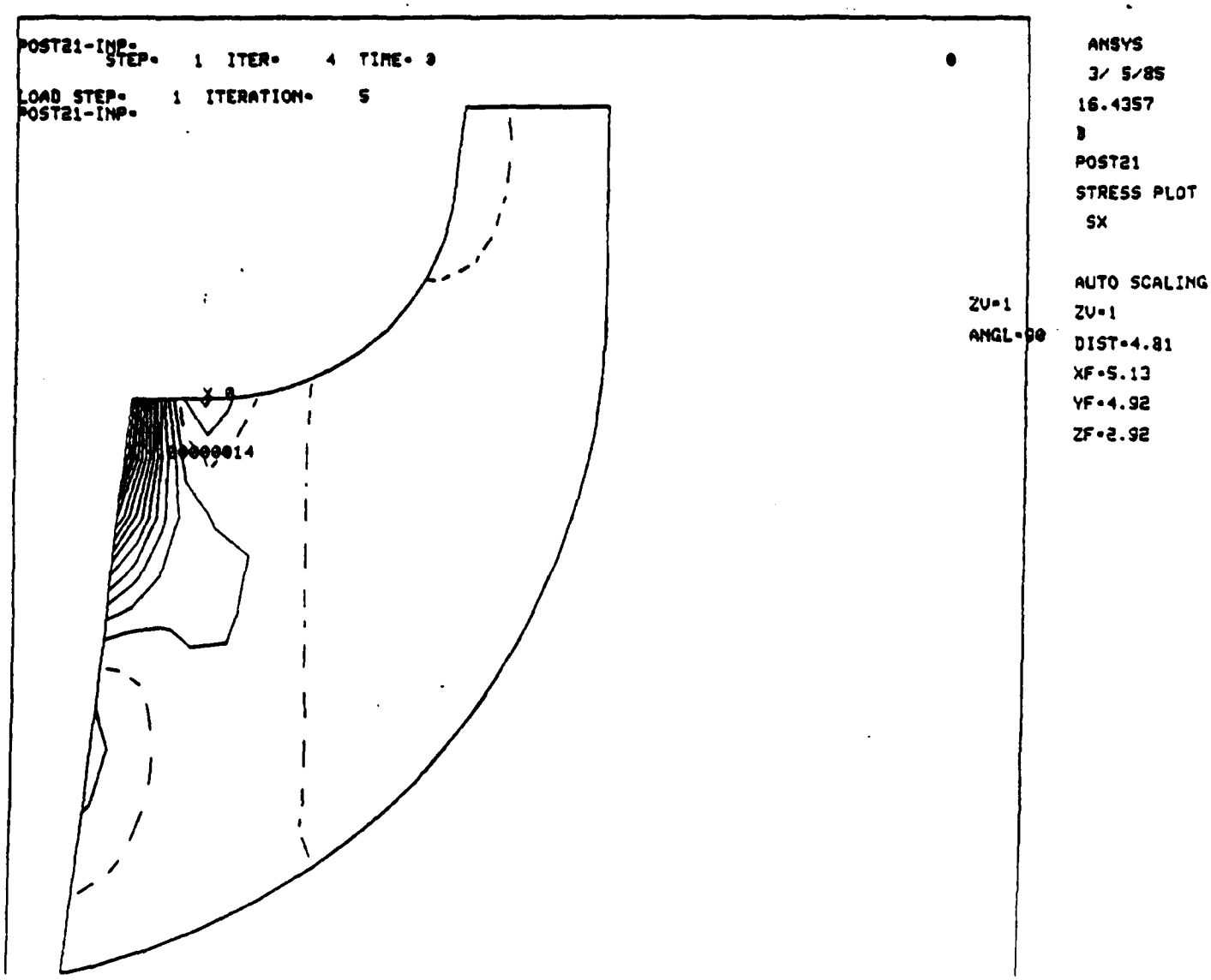

Figure 20. Displacement Contour Plot for Fourth Mode. (17263 Hz)
Predicted by ANSYS Modeling

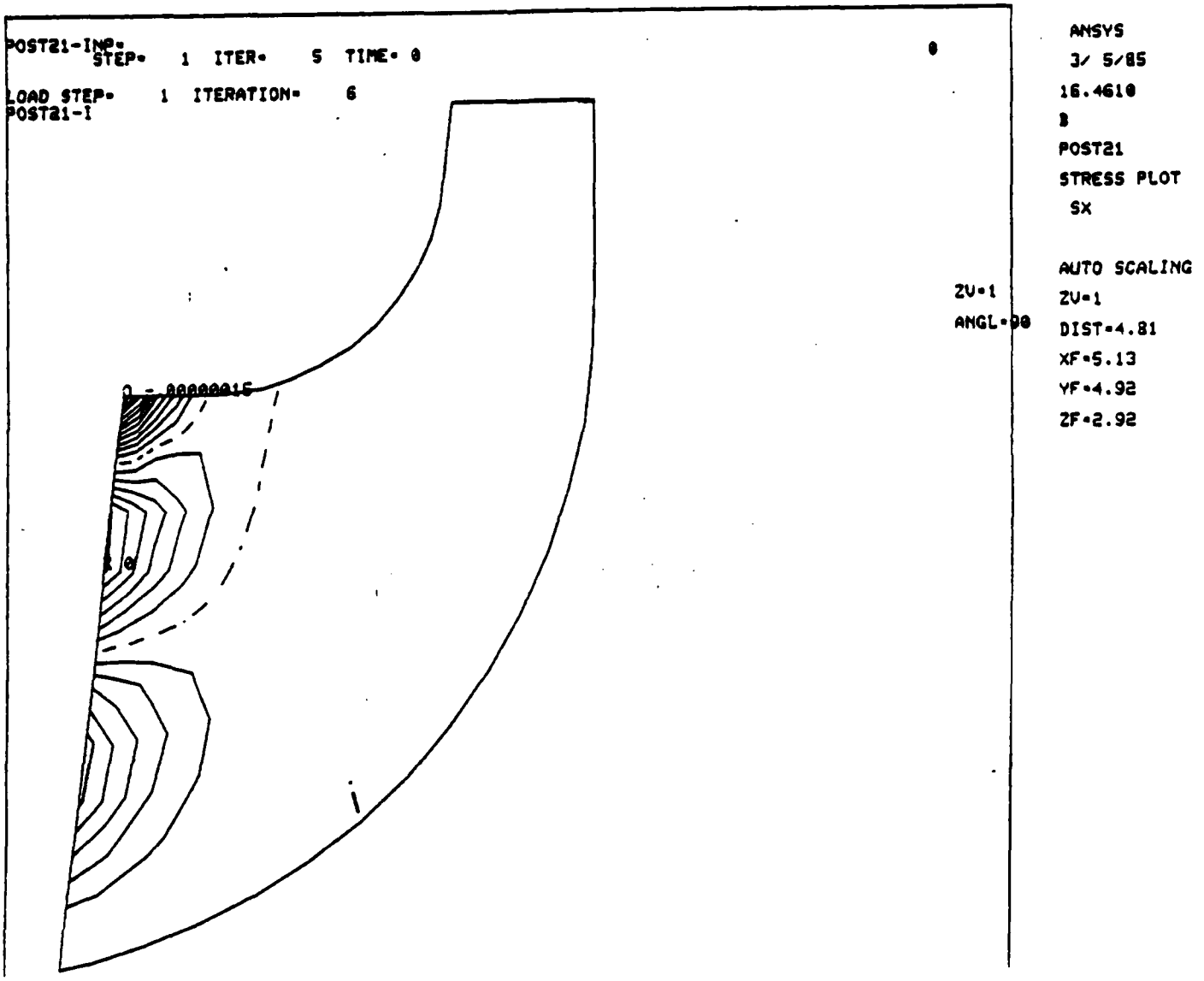

Figure 2E. Displacement Contour Plot for Fifth Mode (18816 Hz)
Predicted by ANSYS Modeling

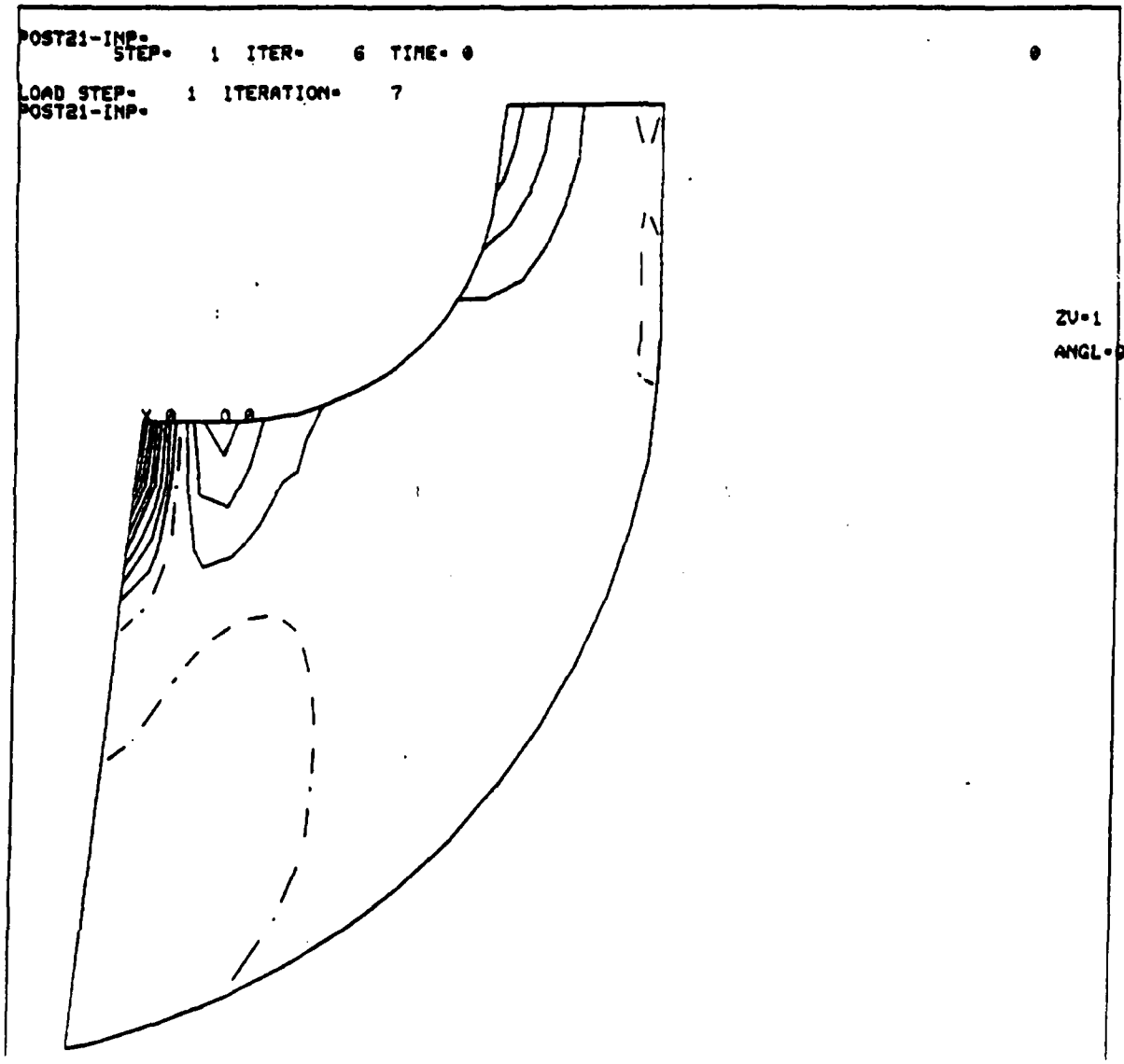

Figure 2F. Displacement Contour Plot for Sixth Mode (21008 Hz)
Predicted by ANSYS Modeling

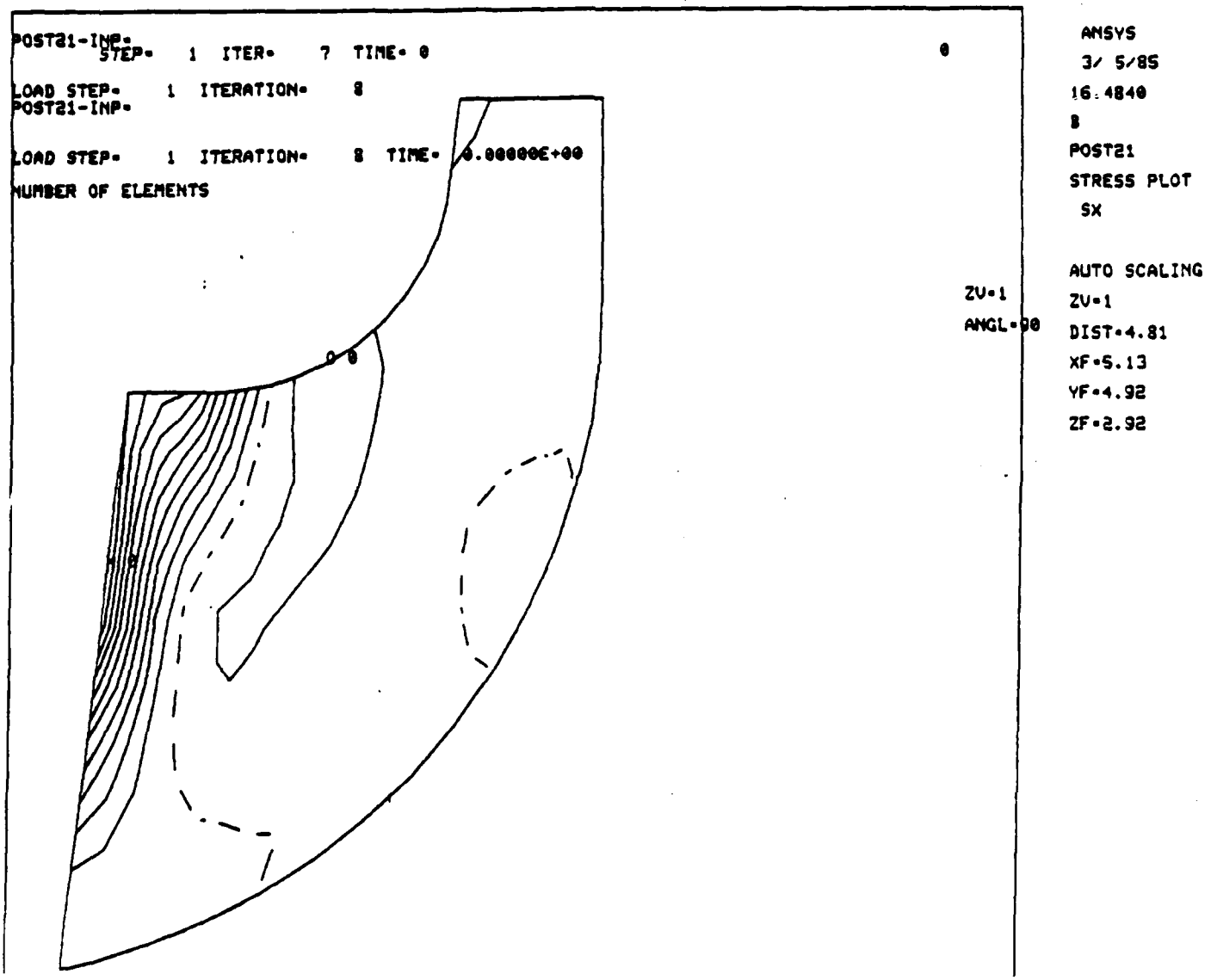

Figure 2G. Displacement Contour Plot for Seventh Mode (24407 Hz)
Predicted by ANSYS Modeling

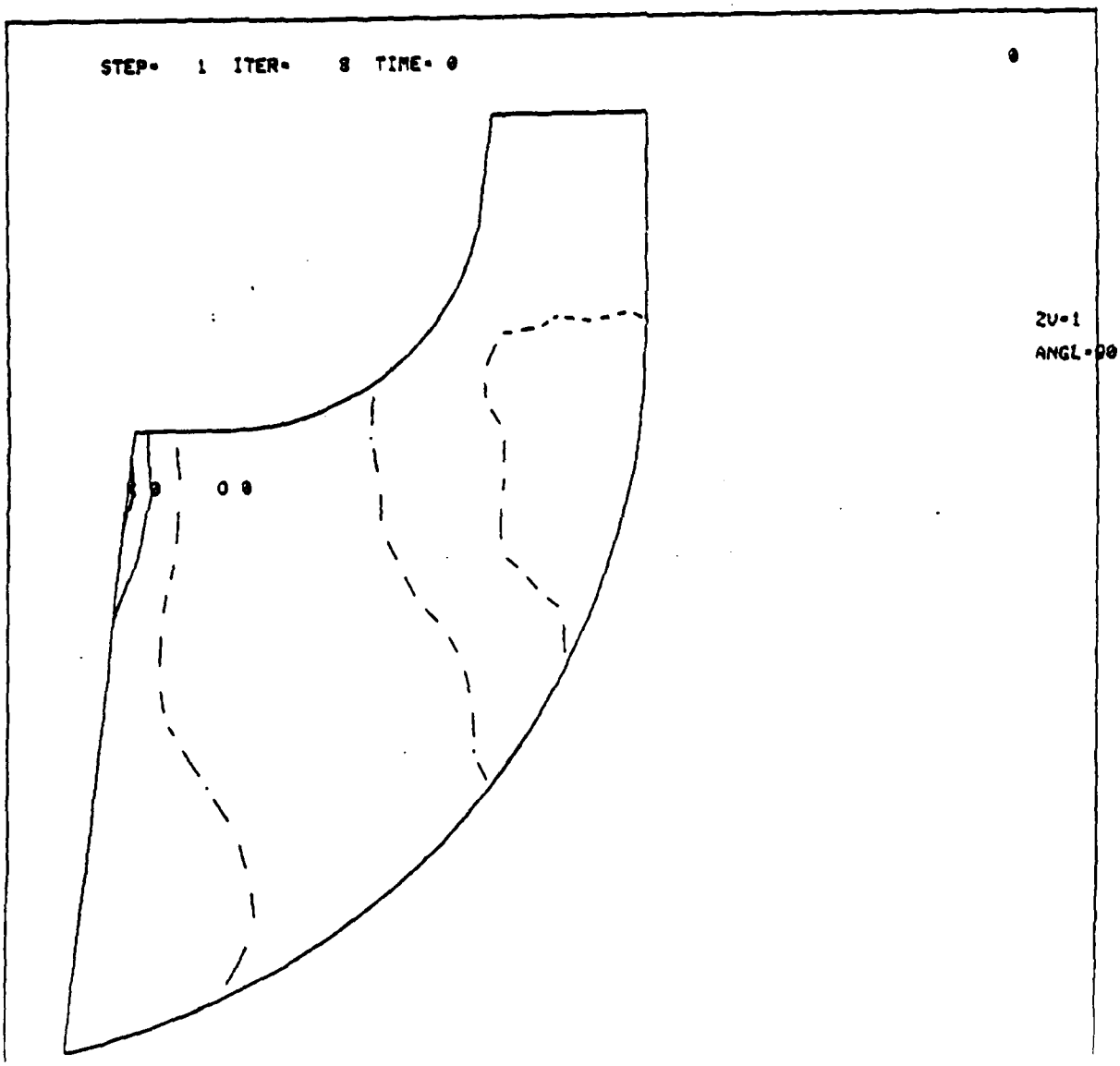

Figure 2H. Displacement Contour Plot for Eighth Mode (16715 Hz) Predicted by ANSYS Modeling

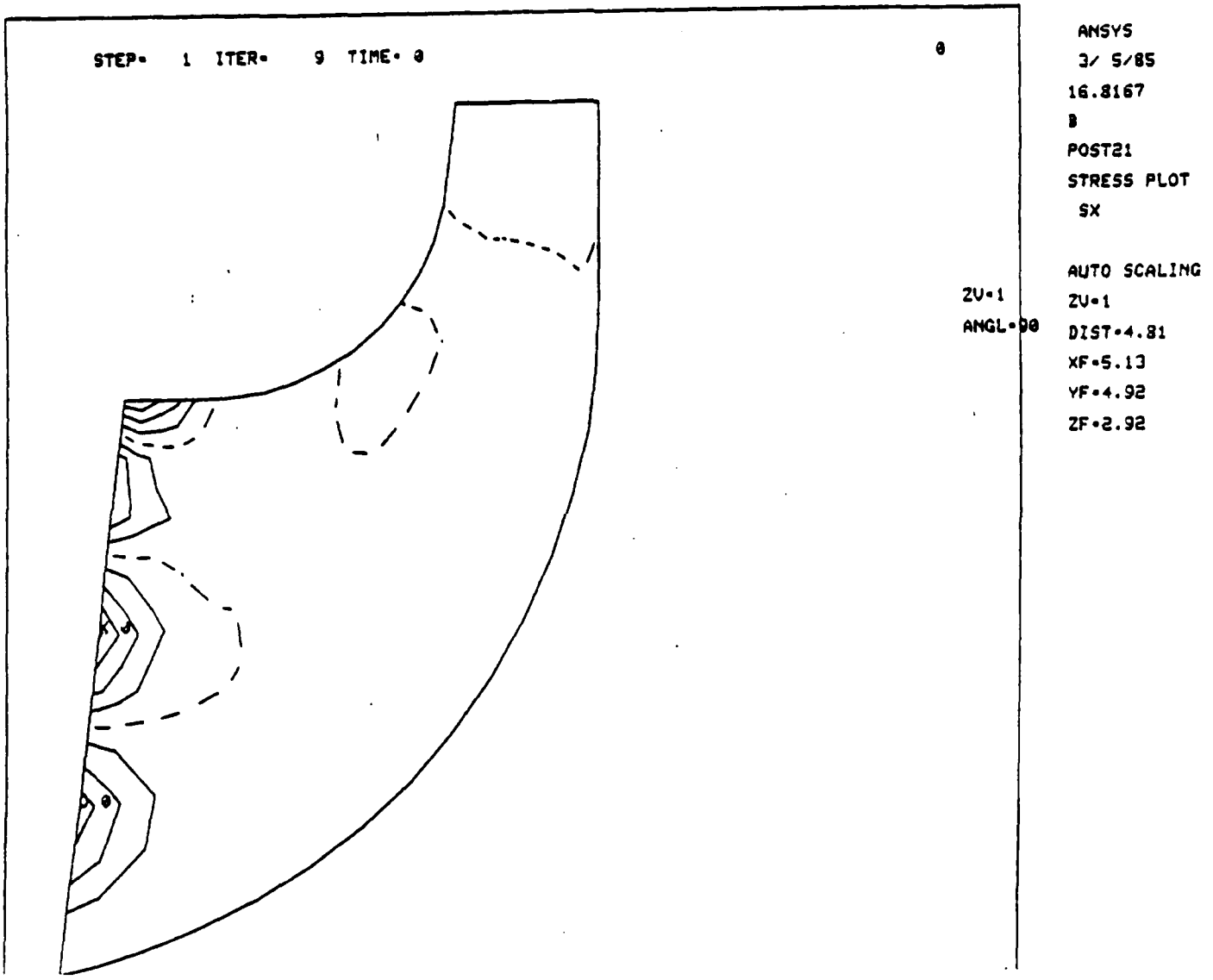

Figure 21. Displacement Contour Plot for Ninth Mode (32309 Hz)
Predicted by ANSYS Modeling

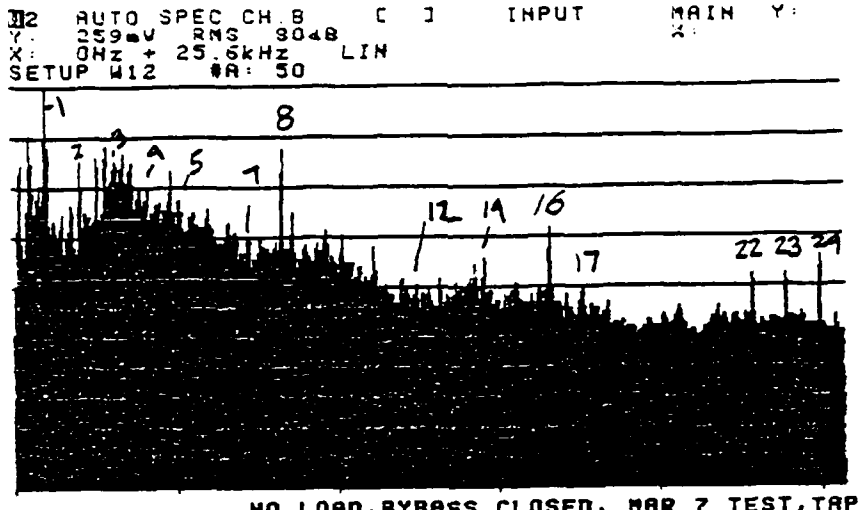

NO LOAD,BYBASS CLOSED, MAR 7 TEST,TAPE COUNT=1200
CH A=CH 2,CH B=CH 3 FILE 3

1

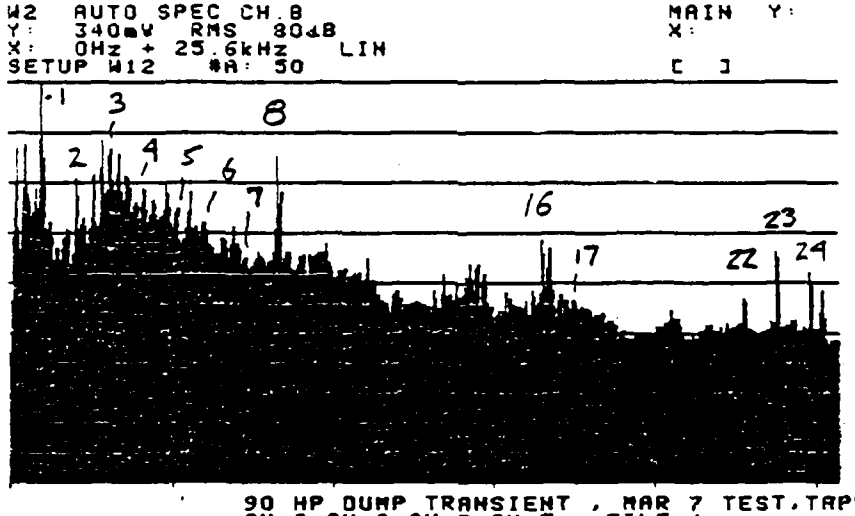

90 HP DUMP TRANSIENT , MAR 7 TEST,TAPE COUNT=1800
CH A=CH 2,CH B=CH 3 FILE 4

1

Figure 3. Vibration Tracing of T-62T-40-1 Turbine Engine:
a) No Load Condition
b) Full Load Condition

1.7 TURBINE WHEEL BURST TEST

As required by Contract N00019-80-G0603, a spin-to-burst test has been conducted on a corrosion resistant turbine wheel P/N 163352-1, S/N 1653-H171 to establish the failure mode.

The spin-to-burst was conducted in incremental steps of 100 percent, 110 percent, 120 percent, 125 percent, 130 percent, 135 percent, 140 percent, 145 percent, and burst speed. The turbine wheel tip diameter, exducer diameter, and bore diameter were measured prior to the initial spin and following each incremental spin as shown in Figure 4. The average growth values for these measurements are pictured in Figure 4.

The turbine wheel burst at 95,090 RPM, or 154.4 percent speed. It burst in a rim-shed failure mode with the largest remaining segment weighing 931gm. The wheel in the "as machined" condition weighs 1.798 Kg. Photographs 1 through 6 show the turbine wheel before and after the burst test.

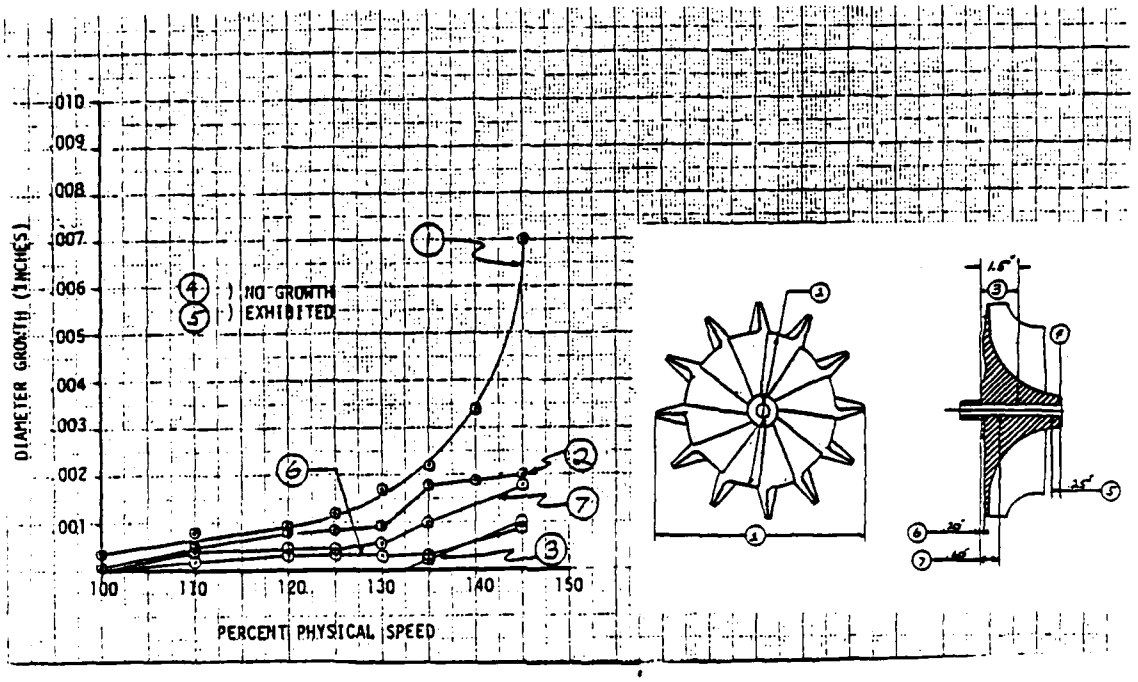

Figure 4. Turbine Wheel 163352-1 S/N 1653-H171
Diameter Growth versus Percent Speed
100 Percent Speed - 61,565 RPM

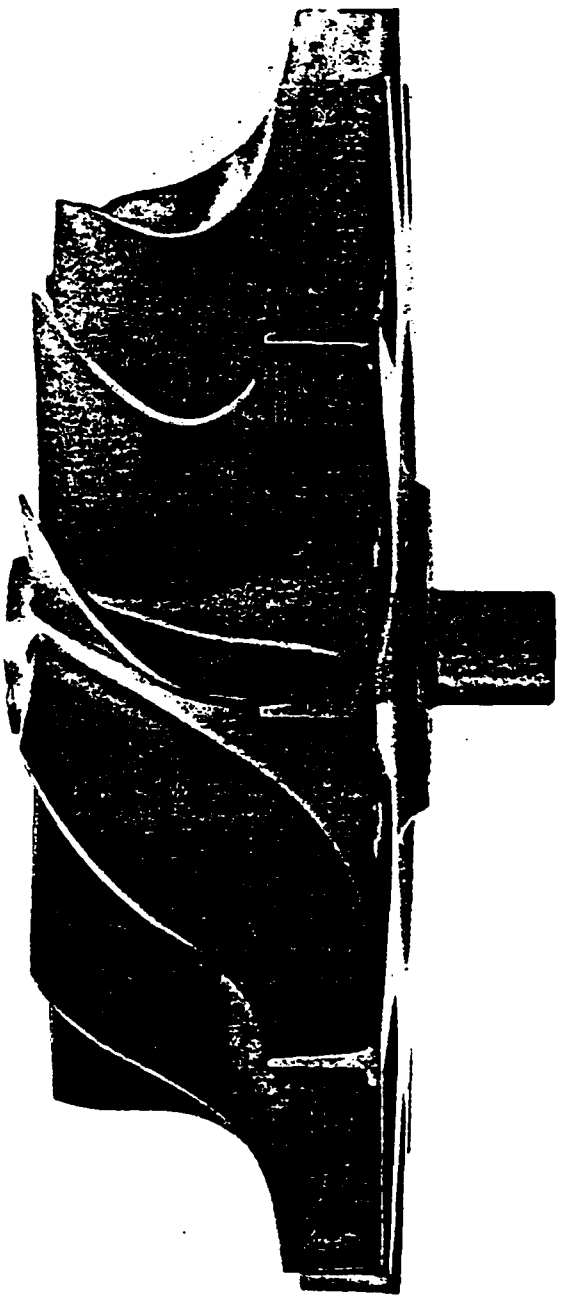

Photograph 1. Turbine Wheel Prior to Burst Test

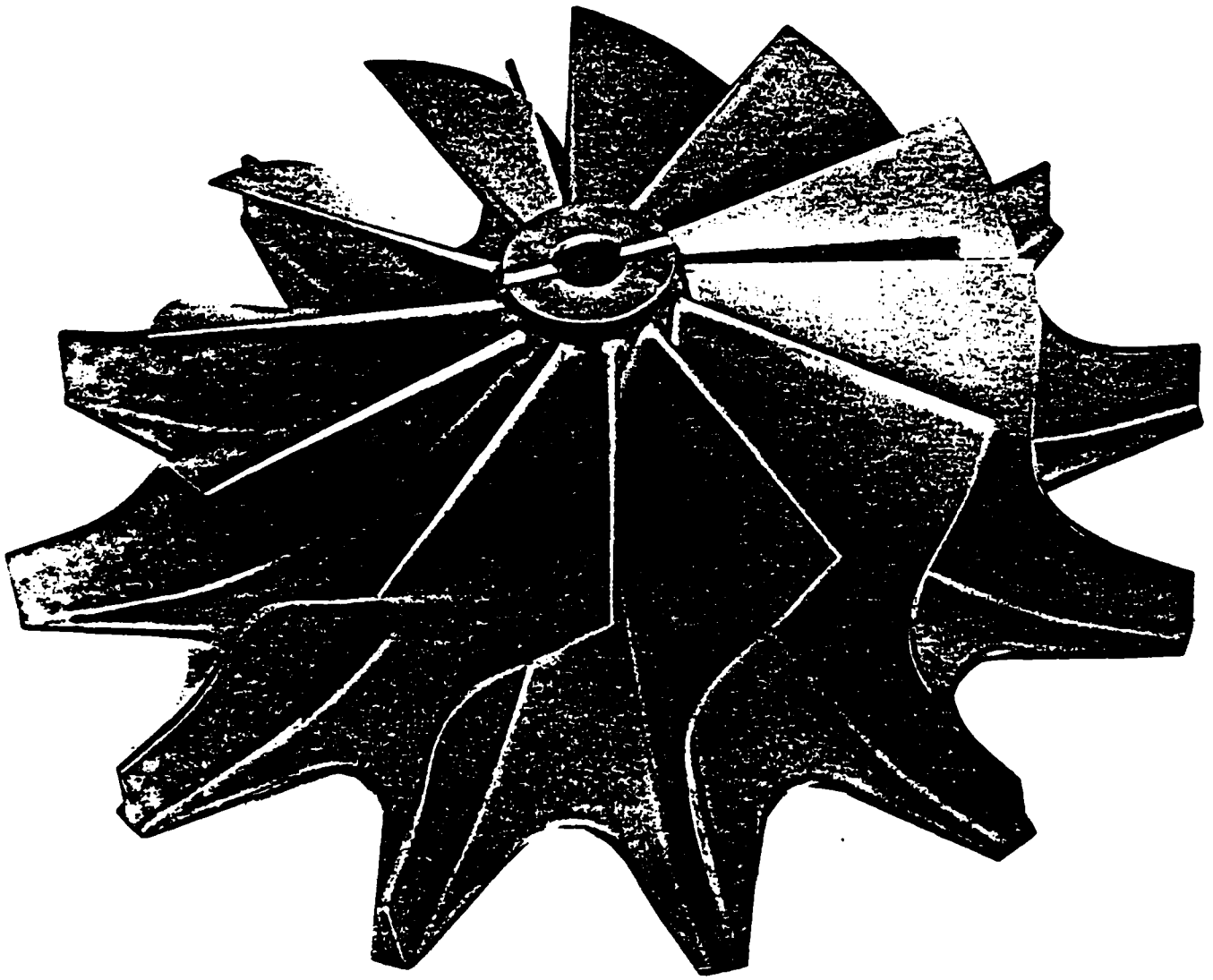

Photograph 2. Turbine Wheel Prior to Burst Test

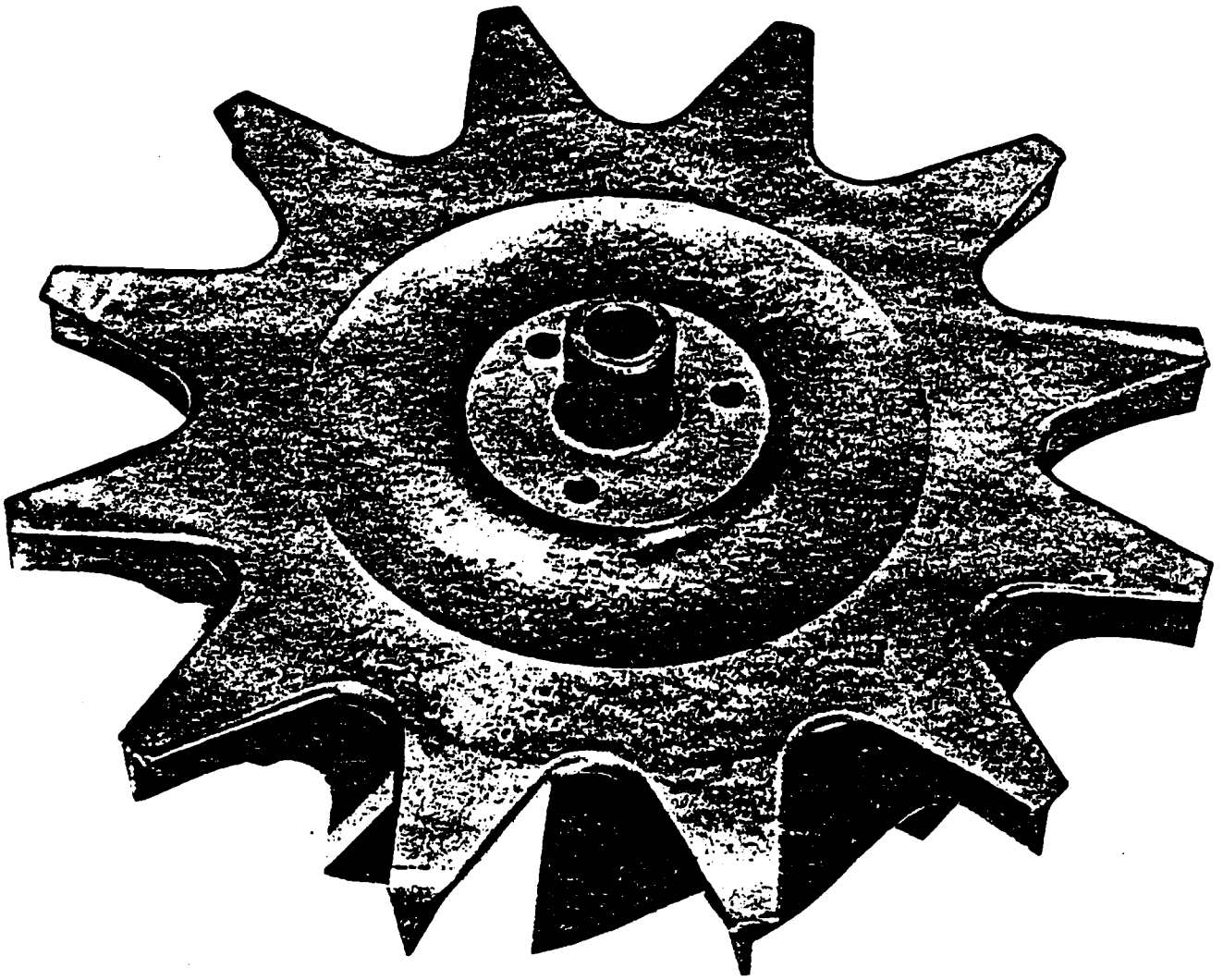

Photograph 3. Turbine Wheel Prior to Burst Test

Photograph 4. Turbine Wheel After Burst Test

Photograph 5. Turbine Wheel After Burst Test

Photograph 6. Turbine Wheel After Burst Test

1.8 MAR-M247 GX MATERIAL TEST PROGRAM

1.8.1 Summary

The purpose of the alternate material turbine wheel program was to replace the current INCO 713LC used in the T-62T-40-1 turbine wheel with an alloy that is more resistant to hot corrosion (sulfidation). A preliminary investigation identified two candidate materials which exhibited good hot sulfidation resistance, IN-792 and MAR-M247. Since both materials exhibited good hot sulfidation resistance, the materials were compared using fatigue strength and stress rupture strength as criteria. Results of initial testing indicated the MAR-M247 to be superior in stress rupture strength and the IN-792 to be superior in fatigue strength. It appeared possible to improve the fatigue strength of the MAR-M247 through heat treatment so the MAR-M247 was chosen for further development. The MAR-M247 was also better suited to casting processes.

The development of the heat treatment for the MAR-M247 included optimizing both the solution heat treatment and the aging heat treatment. This would improve the fatigue strength by improving the tensile strength and by minimizing the loss in ductility. MAR-M247, being a nickel-base superalloy, is primarily strengthened by precipitation of the gamma prime phase from a saturated solid solution. Therefore, the function of the solution heat treatment is to put as much of the gamma prime phase into solution as possible so that it can subsequently be precipitated out in the most desirable grain size and distribution. The effectiveness of the solution heat treatment is determined by the solution temperature. The optimum solution temperature is identified as the highest temperature that will not produce incipient melting. The onset of incipient melting was observed to occur at 2275°F. As a result, the optimal solution temperature was determined to be 2250°F.

The aging heat treatment allows for the precipitation of the gamma prime strengthening phase from the super-saturated solid solution. The aging temperature and time determine the final gamma prime morphology. The optimized aging heat treatment must be determined iteratively and is based on

the property-microstructure correlation observed after various aging treatment trials. Tensile testing the material at 1000°F after various aging treatments served as the basis for the evaluation of the aging trials. The results of the testing are tabulated below:

	UTS (ksi)	YS(ksi)	Elong(%)	RA (Z)
2250°F/2 hrs. + 1400°F/20 hrs.	142.6	126.7	4.3	10.6
2250°F/2 hrs. + 1600°F/20 hrs.	142.8	130.2	2.9	9.7
2250°F/2 hrs. + 1800°F/20 hrs.	143.3	123.0	4.5	9.9
2250°F/2 hrs. + 1900°F/20 hrs.	141.7	123.8	5.6	11.0
1600°F/20 hrs	131.2	103.8	7.6	12.1

The revised heat treatment was then determined to be
2245 $\pm$ 20°F/2 Hrs + 1900 $\pm$ 25°F/20 Hrs.

The solution heat treatment was lowered to 2245°F to facilitate processing (i.e., minimum allowable temperature 2265°F).

To confirm the improvement of the heat treatment, stress rupture and low cycle fatigue testing were performed. Results of these tests confirm that the fatigue strength can be improved with no loss in stress rupture life as shown in Figures 5 and 6. In each case, the results are shown with respect to the data obtained from MAR-M247 GX in the 1600°F/20 hr age heat treat condition.

With the establishment of the revised heat treatment for MAR-M247 GX, a test program was developed to qualify the material for use in gas turbine applications at Turbomach. The test program included an evaluation of the hot corrosion resistance of MAR-M247 GX, with the revised heat treatment, in comparison to several other nickel-based superalloys. In addition, a full material test program was developed which included:

- o Tensile testing
- o Creep rupture testing
- o High cycle fatigue testing
- o Low cycle fatigue testing
- o Fracture toughness testing
- o Fatigue crack growth rate testing

A summary of the test results follows.

STRESS RUPTURE
MAR-M247GX
TEST LABS: DICKSON (6 POINTS) AMS (6 POINTS)

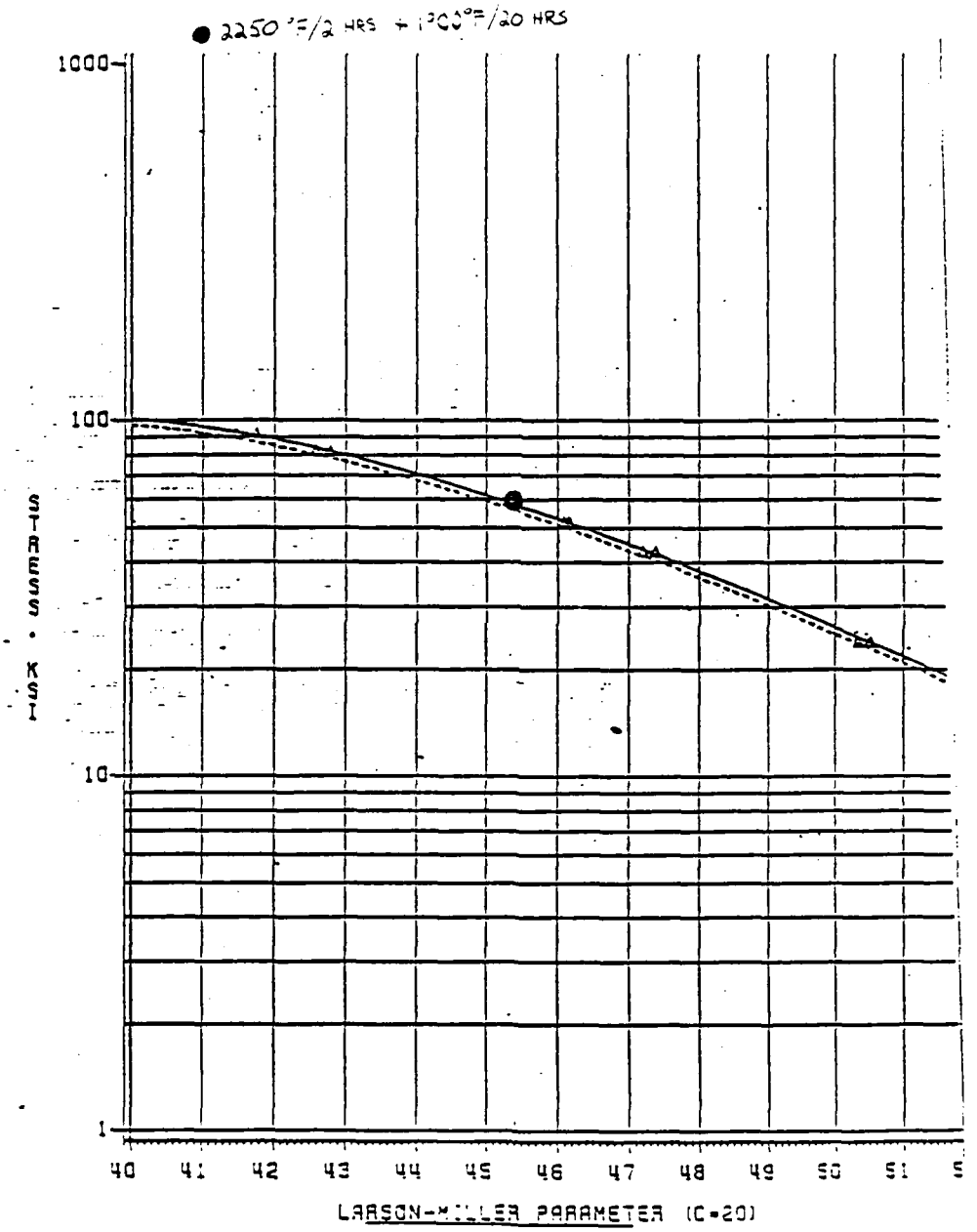

Figure 5. Larson-Miller Plot for MAR-M247 GX Stress Rupture

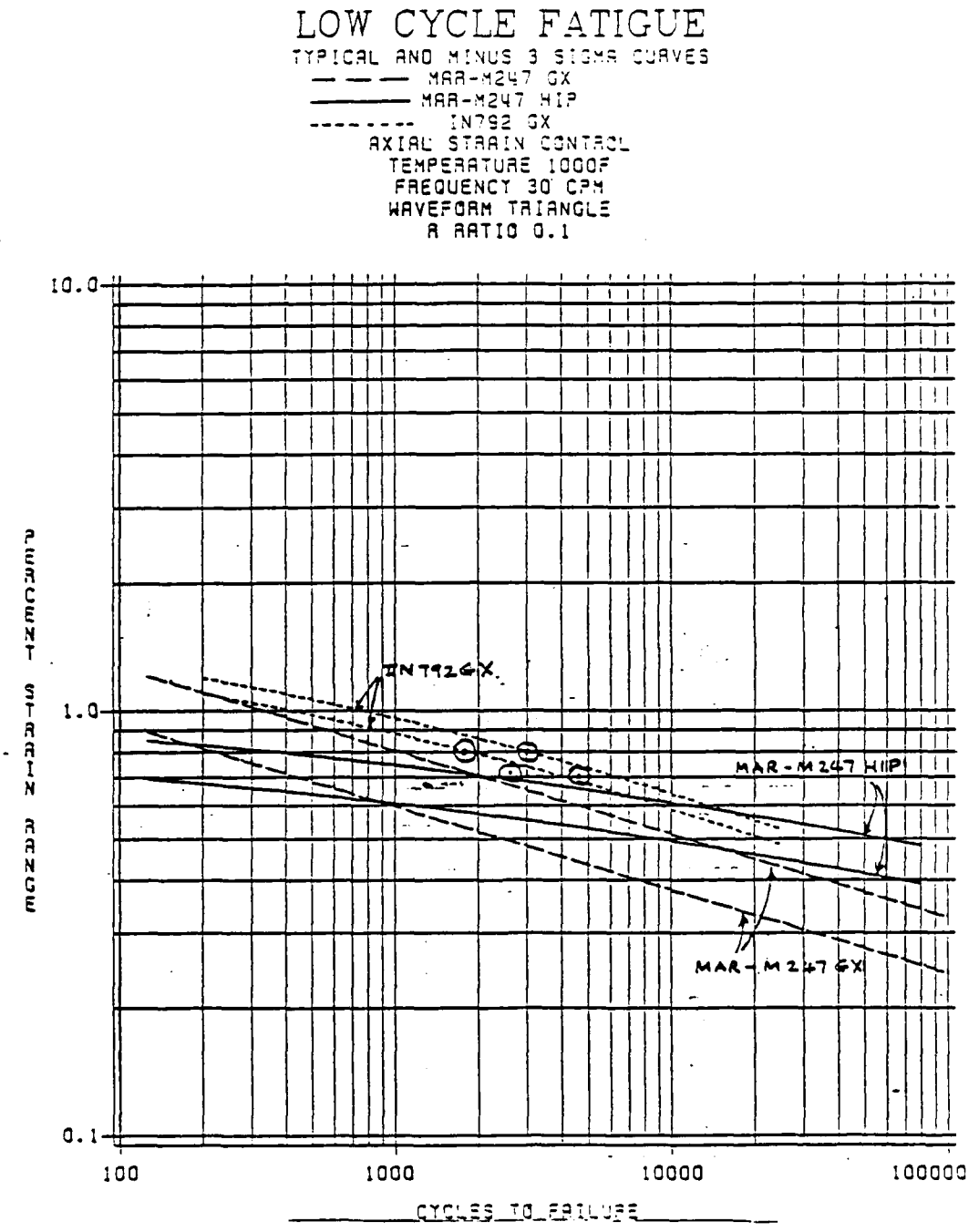

Figure 6. Comparison Plot of Low Cycle Fatigue Behavior
(MAR-M247 GX, MAR-M247 HIP, IN 792 GX)

1.8.2 SULFIDATION TEST

To assess any possible detrimental effects associated with either using MAR-M247 GX or the revised heat treatment, a test program to determine the material's sulfidation resistance in relation to other nickel-based superalloys was carried out. The program consisted of furnace testing the materials at the conditions outlined in Table III.

Table III. Sulfidation Testing Materials and Conditions

Materials

MAR-M247 GX Improved H.T.
MAR-M247 GX Aged Only H.T.
IN-713 LC
MAR-M 421
IN-792 Mod 5A

Conditions

1. 95% Na_2SO_4 5% NaCl

   1 mg/cm^2 Salt Deposit

   1500°F

   Approximately 24 Hours Per Exposure

2. 100% Na_2SO_4

   1 mg/cm^2 Salt Deposit

   1650°F

   Approximately 24 Hours Per Exposure

After each furnace exposure, the specimens were washed with deionized water and wire brushed to remove any spalled oxide. Specimens were then weighed and recoated with 1 mg/cm^2 salt. Testing was terminated after 534 hours.

The results of the sulfidation testing are summarized in Table IV and are shown on the weight loss curve (Figures 7 and 8) for conditions 1 and 2, respectively. MAR-M421 is regarded as a hot corrosion resistant material. This is primarily due to its high chromium content. IN-713LC alloys generally perform poorly under conditions that promote hot corrosion even though the alloys have excellent resistance to simple oxidation. Both the MAR-M247 and the IN-792 alloys are designed to maximize the high-temperature mechanical properties while sacrificing some of the oxidation and corrosion resistance (Figure 8). This general trend is also maintained for the low temperature condition 1, shown in Figure 7. However, the MAR-M247, MAR-M 421, and IN-792 all showed excellent long-term resistance. A significant improvement in the corrosion resistance appears to have resulted from the revised heat treatment. This was possibly due to the greater solutioning of the lower melting eutectic phase(s) in the cast microstructure. Further evaluation of this effect, including additional corrosion tests and surface penetration measurements by metallography, is recommended before final conclusions are reached.

Turbomach
division of Sundstrand Corporation
4849 Ruffin Road, P.O. Box 85757, San Diego, California 92138-5757
FSCM 55820

Table IV
Summary of Sulfidation Results

Condition 1	Corrosion Area (cm^2)	Cumulative Weight Change (mg/cm^2) per Exposure (Hour)															
		24	46	66	86	100	120	144	168	192	213	259	329	351	410	480	534
MAR-M421	3.25	-2.1	-0.4	-2.1	-3.9	-9.1	-10.5	-12.6	-13.2	-13.8	-15.4	-19.1	-26.6	-17.0	-27.6	-38.3	-47.1
MAR-M247 New Heat Treat	3.29	-0.8	+0.4	+0.9	+1.6	+2.5	+3.1	+4.2	+3.9	+7.4	+6.3	+10.2	+11.8	+22.1	+70.8	+88.7	+101.7
MAR-M247 Conventional H.T.	3.29	-1.7	+2.1	+4.2	-5.5	-32.7	-33.9	-76.6	-122.7	149.9	226.2	-	-	-	-	-	-
IN-792 Mod 5A	2.72	-2.2	-1.3	-1.3	-0.7	-0.6	+0.33	+0.7	+11.8	+0.37	+0.81	+1.1	+3.3	+11.9	+8.2	-31.2	-31.1
IN-713 L.C.	1.82	-1.9	-1.6	-2.9	-2.5	-19.7	-26.8	-50.4	-151.8	-211.8	-	-	-	-	-	-	-

Condition 2	Corrosion Area (cm^2)	Cumulative Weight Change (mg/cm^2) per Exposure (Hour)															
		24	46	66	86	100	120	144	168	192	213	259	329	351	410	480	534
MAR-M421	3.26	-0.4	0	+0.1	0	0	+0.15	-0.22	-0.2	+1.7	+4.6	+10.4	+20.1	+10.4	-	-	-
MAR-M247 New H.T.	3.27	+1.1	+7.7	-10.6	-28.6	-47.5	-70.5	-155.2	-176.4	-213.7	-	-	-	-	-	-	-
MAR-M247 Conventional H.T.	3.29	-0.5	-23.8	-234.1	-	-	-	-	-	-	-	-	-	-	-	-	-
IN-792 Mod 5A	3.06	-0.5	+10.2	+11.5	+6.3	-12.2	-29.8	-34.7	-46.7	-76.0	-76.0	-114.8	-19[illegible].7	-236.2	-	-	-
IN-713 L.C.	1.82	-8.5	-20.6	-172.5	-389.3	-	-	-	-	-	-	-	-	-	-	-	-

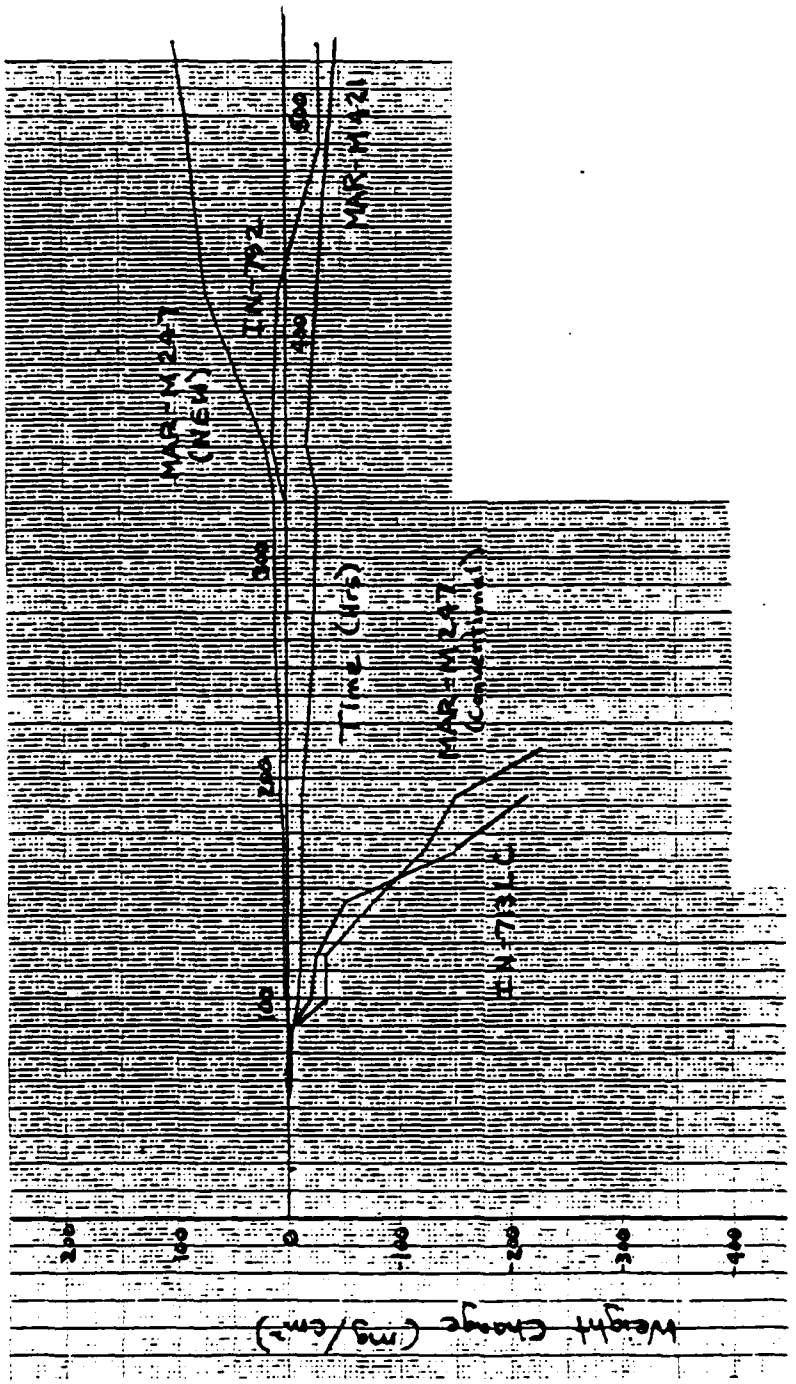

Figure 7. Sulfidation Test Results - Condition 1 - 95% Na_2SO_4, 5% NaCl, 1 mg/cm^2 Salt Deposit, 1500°F.

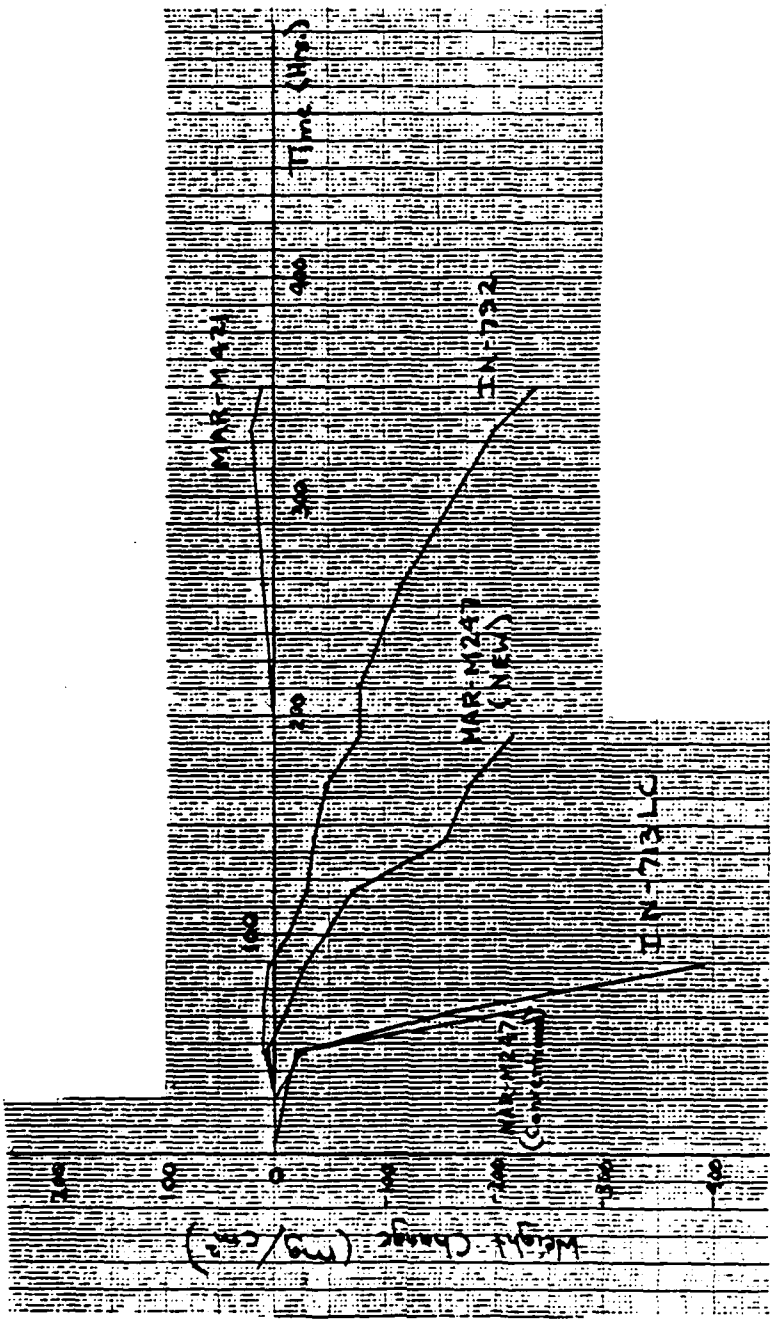

Figure 8. Sulfidation Test Results - Condition 2 - 100% Na_2SO_4, 1 mg/cm^2 Salt Deposit, 1650°F.

1.8.3 Mechanical Test Program

An outline of the mechanical test program is given in Table V.

Table V. Mechanical Test Program

1. Tensile (12 tests)

   R.T., 800, 1000, 1200, 1400, 1600°F

2. Creep-Rupture (27 tests)

Temperature	Stress Level (ksi)	Expected Life (hr.)
1400°F	95	100
	85	500
	80	1000
1600°F	75	10
	60	100
	42	1000
1800°F	40	10
	28	100
	20	500

3. High Cycle Fatigue (axial-axial) (42 tests)

   1200°F @ R = -1.0, 0.25 and 0.1
   1500°F @ R = -1.0, 0.25 and 0.1
   R.T. @ R = -1.0

4. High Cycle Fatigue (shaker table) (8 tests)

   R. T. @ R = -1.0

5. Low Cycle Fatigue (16 tests)
   (Smooth Bar Testing)
   R.T., 500°F @ R = 0.1
   Strain Range 0.5 - 1.0%

6. Crack Propagation

   1100°F @ R = -0.5

(Continued next page)

Table V. Mechanical Test Program (Continued)

7. Holographic Analysis

-Back Face, Rim, Blades
-0-20 HTZ

(NOTE: $R = \frac{Emin}{Emax}$ or $A = \frac{Emax-Emin}{Emax+Emin}$)

A summary of the mechanical test results is given below.

Tensile Test

Tensile testing of the MAR-M247 GX material was performed in both the aged only and revised heat treatment conditions. Room temperature and elevated temperature tests were performed. The results of the average of two specimens are shown in Table VI. A plot of the tensile properties versus test temperature is shown in Figure 9.

Table VI. Summary of Tensile Testing Results

	Room Temperature	800°F	1000°F	1200°F	1400°F	1600°F
Aged only heat treatment						
Tensile strength (ksi)	136.0	137.0	131.2	130.0	--	115.4
0.2% Yield stress (ksi)	115.0	112.0	103.0	103.0	--	99.0
% Elongation	9.4	7.8	7.6	4.7	--	7.75
Revised heat treatment						
Tensile strength (ksi)	144.0	142.4	141.7	138.4	133.8	120.5
0.2% Yield stress (ksi)	122.7	127.0	123.8	122.9	126.5	118.8
% Elongation	8.8	5.8	5.6	4.8	2.9	1.8

Note: Aged only H.T. HIP + 1600°F/20 hours
Revised H.T. HIP + 2245°F/20 hours + 1900°F/20 hours

The data clearly shows that the revised heat treatment improves both tensile and yield strengths with a reduction in tensile elongation. The aged only heat treated MAR-M247 shows the commonly observed dip in

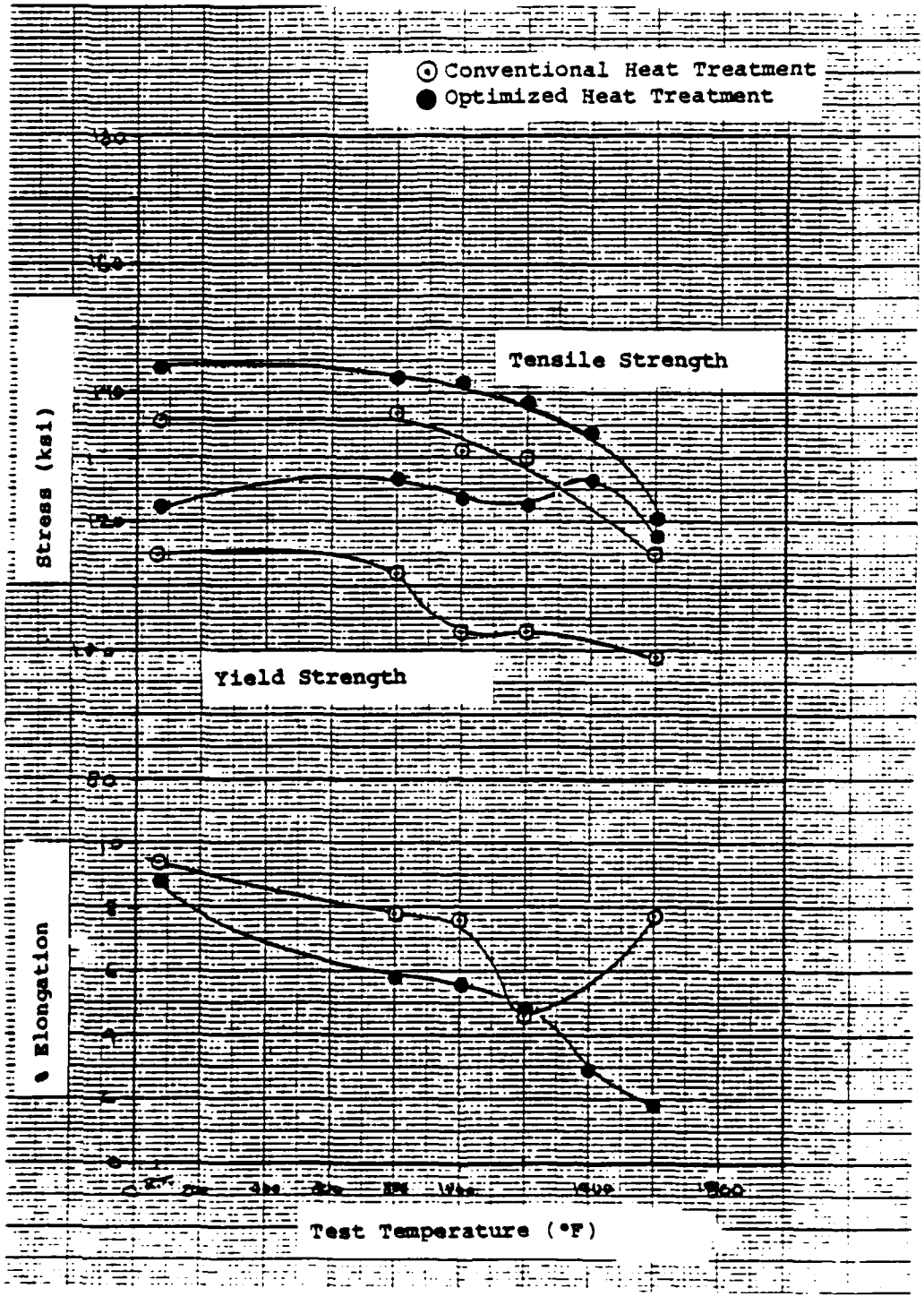

Figure 9. Results of Tensile Test Program.

tensile elongation at 1400°F. The revised heat treatment, however, shows continuous decrease in elongation with increasing test temperatures. Although at a test temperature of 1200°F, the elongation for both heat treatments was found to be equal with a 20 percent increase in the yield strength and a 6 percent increase in the tensile strength.

Creep Rupture Test

A total of 24 creep rupture specimens were tested to failure. In each case, extensometers were attached to the specimens so that creep curves could be generated. Tests were conducted at 1400, 1600, and 1800°F over a variety of loading levels in order to obtain rupture lines between 10 and 1000 hours nominal. The results of the test program are shown in Table VII. The results are also shown on the Larson-Miller parameter plot (C=20), Figure 10. The data is shown on a plot generated from aged only heat treated material, and the solid symbol is from the initial test results. In general, the stress rupture data from the material receiving the revised heat treatment correlate well with that of the aged only heat treated material. The new heat treatment may result in a slight drop in rupture life at low L-M parameter, i.e. the low-temperature tests. However, it appears to be no more than 5 ksi. Also, at 1400 and 1600°F, the rupture ductility has been reduced. Further heat treatment development is recommended to avoid this ductility degradation.

Table VII. MAR-M247 GX Creep Rupture

SPECIMEN			CONDITIONS		RESULTS			
NO.		S/N	TEMP.	STRESS	TIME TO RUPTURE (HOURS)	LARSON-MILLER PARAMETER C = 20	TOTAL ELONG.	REDUCT. IN AREA
1	C-7	D-470	1400	95	58.9	(40.5)	0.9%	0.7%
2	C-3	3-A63	1400	95	40.9	(40.2)	1.5%	4.7%
3	D-1	3-A66	1400	95	20.8	(39.7)	1.4%	6.0%
4	C-1	3-A62	1400	85	570.5	(42.3)	1.66%	3.5%
5	D-2	3-A72	1400	85	122.5	(41.1)	0.94%	2.9%
6	D-3	3-A66	1400	85	56.0	(40.5)	1.4%	2.7%
7	C-2	3-A62	1400	80	1730.2	(43.2)	2.6%	4.2%
8	D-4	3-A64	1400	80	947.0	(42.7)	3.3%	2.5%
9	D-5	3-A73	1400	80	597.6	(42.4)	1.9%	
10	C-4	3-A63	1600	75	4.6	(42.6)	1.36%	5.5%
11	D-6	3-A75	1600	75	6.8	(42.9)	2.5%	2.5%
12	F-11	H-116	1600	75	8.2	(43.1)	2.3%	3.55%
13	C-8	D-470	1600	60	102.7	(45.3)	4.8%	5.7%
14	C-9	3-A59	1600	60	105.2	(45.4)	4.66%	5.0%
15	D-7	3-A73	1600	60	62.9	(44.9)	4.0%	4.3%
16	F-32	H-116	1600	42	1519.0	(47.8)	8.6%	9.8%
17	D-8	3-A64	1600	42	1583.3	(48.9)	10.6%	13.9%
18	D-9	3-A73	1800	42	933.3	(47.3)	6.4%	6.6%
19	C-6	3-A65	1800	40	15.7	(47.9)	8.2%	10.0%
20	F-23	H-116	1800	40	14.3	(47.8)	6.4%	9.65%
21	F-24	D-456	1800	28	163.7	(50.2)	8.3%	12.0%
22	D-10	3-A66	1800	28	78.5	(49.5)	6.0%	8.2%
23	C-5	3-A65	1800	25	243.3	(50.6)	9.5%	15.6%
24	C-10	3-A59	1800	20	719.4	(51.7)	9.4%	29.0%

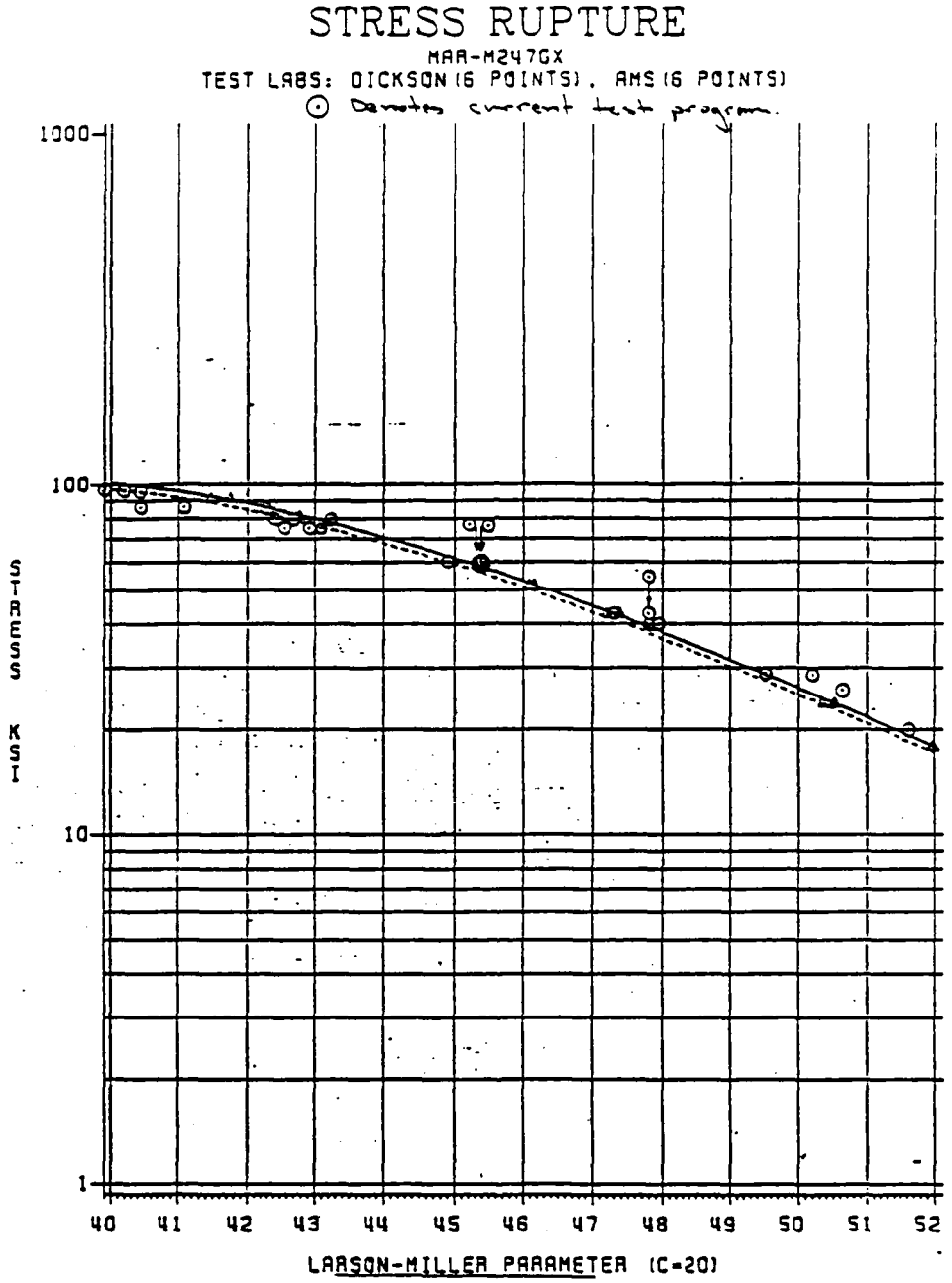

Larson - Miller Plot
for MAR - M 247 HIP
(Typical and minus 3
sigma curves)

Figure 10. Larson-Miller Plot for MAR-M247 HIP Creep Rupture

High Cycle Fatigue (Axial Test)

The High Cycle Fatigue (HCF) test program consisted of seven test conditions with six specimens per condition. The conditions are outlined in Table VIII and range from room temperature to 1500°F and R ratios from -1.0 to 0.25. The HCF results are illustrated in Figures 11 through 15. Figures 11 and 12 and S-N curves at constant temperature and various R ratios. For the curves at either 1200°F or 1500°F, the cycles to failure at constant maximum stress increase with increasing R ratio. Figures 13 through 15 show the effects of temperature on the fatigue life with constant R ratios. It appears that lowering the test temperature tends to increase the fatigue life. This effect, however, appears to diminish at run-out (i.e. 10^7 cycles).

Table VIII. High Cycle Fatigue Test Conditions

Temperature	R Ratio
1200°F	-1.0
1200°F	0.1
1200°F	0.25
1500°F	0
1500°F	0.1
1500°F	0.25
75°F	-1.0

Mode: Axial Load Control
Frequency: 60 Hz
Waveform: Sinusoidal

*R Ratio = $\frac{\text{Min. Stress}}{\text{Max.-Stress}}$

NOTE: Six Specimens Tested per Condition

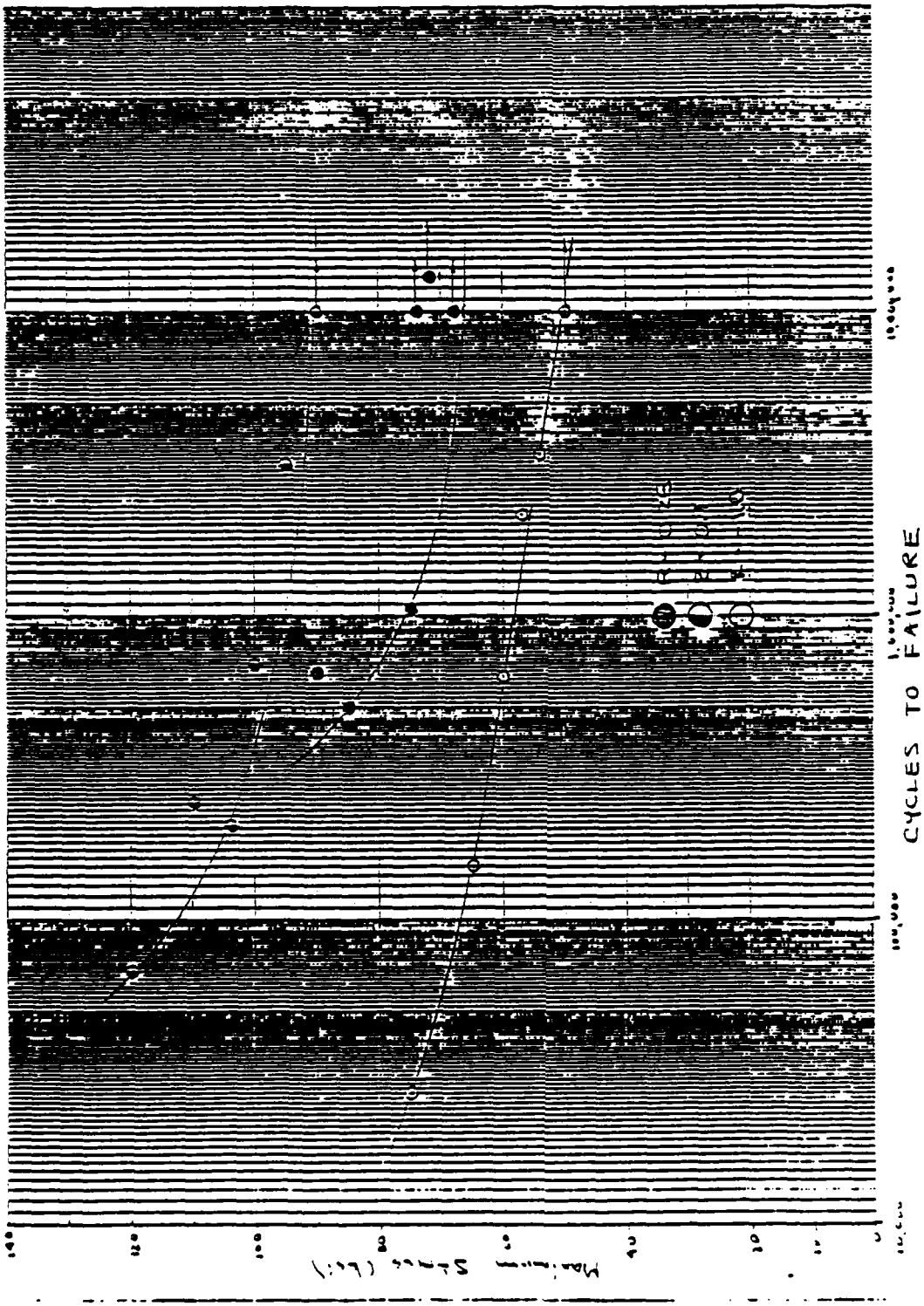

Figure 11. HCF Test Results at 1200°F.

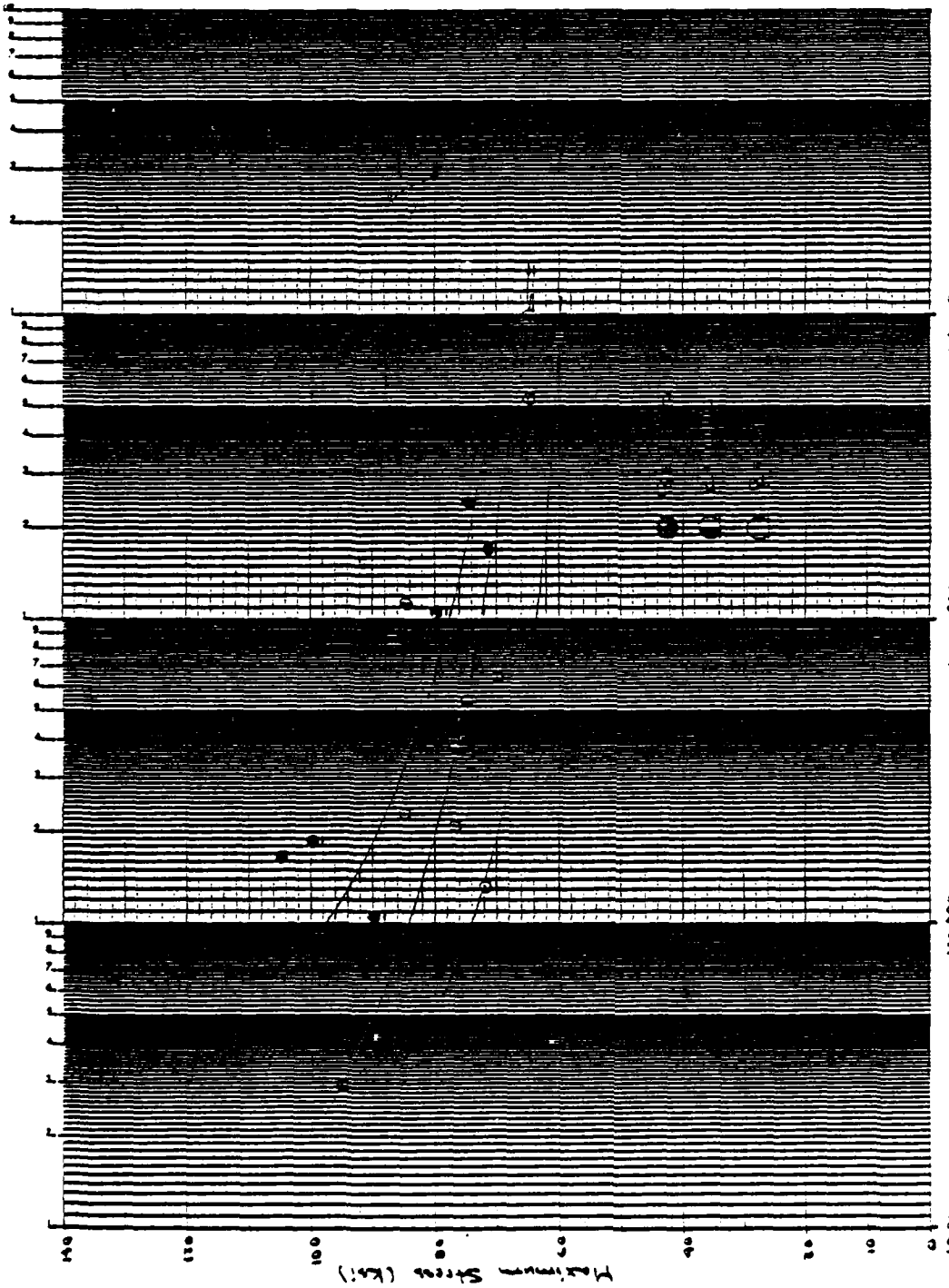

Material: MAR-M-247
Frequency: 60 Hz
Waveform: Sinusoidal

Figure 12. HCF Test Results at 1500°F.

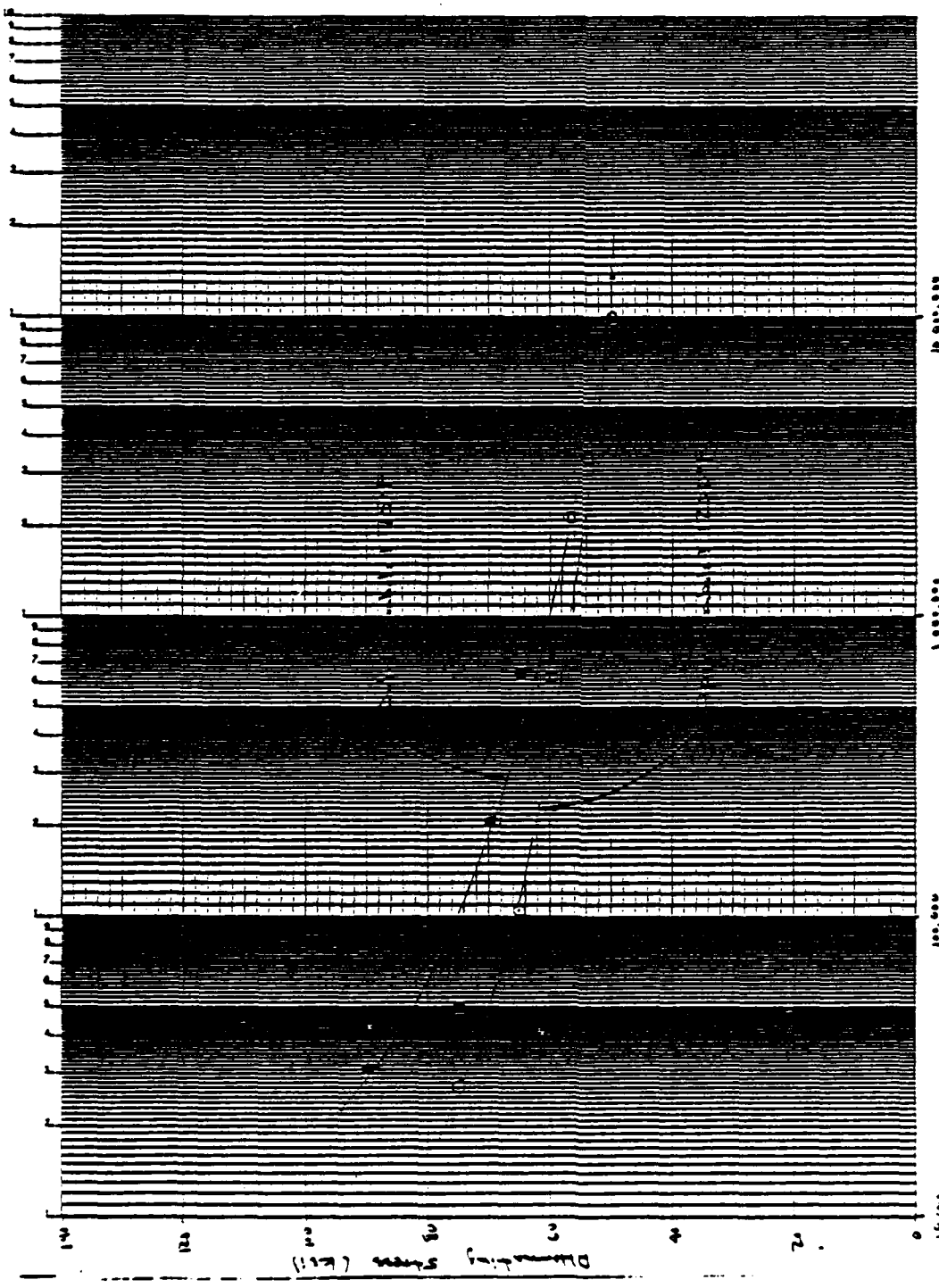

Figure 13. HCF Test Results with Constant R = -1.0 and Temperature Varying.

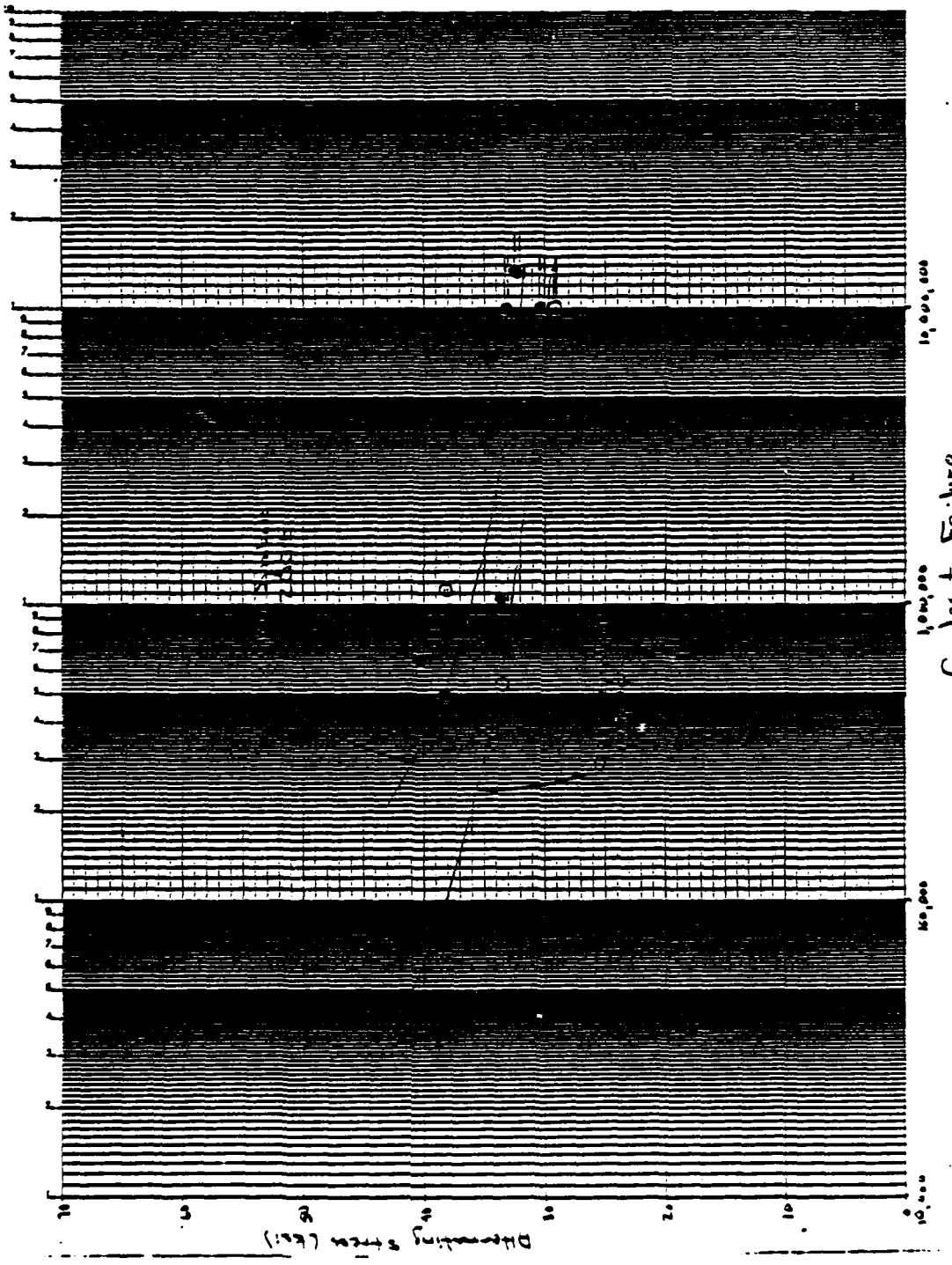

Figure 14. HCF Test Results with Constant R = 0.1 and Temperature Varying.

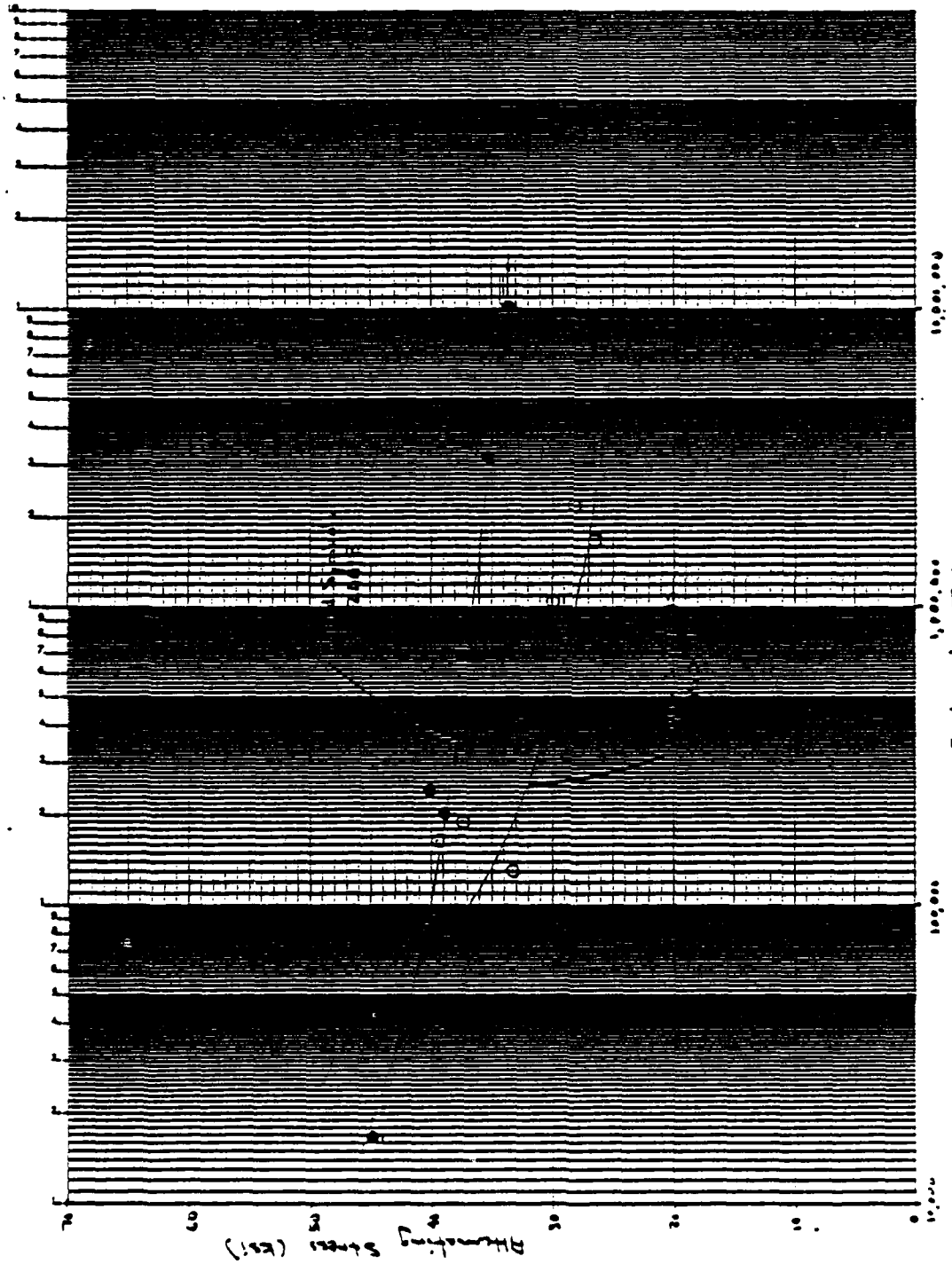

Figure 15. HCF Test Results with Constant R = 0.25 and Temperature Varying.

High Cycle Fatigue (Shaker Table)

Shaker table fatigue testing has proved to be difficult and results obtained are unreliable. The acceleration required to excite a vane is extremely high (in excess of 100 g's), taxing the limit of the shaker table. Several configurations were tried and fatigue cracks initiated, however, the confidence level in the results is very low.

This task has been suspended due to failure of Solar's shaker and reluctance to continue testing with an outside vendor.

Low Cycle Fatigue

Low cycle fatigue testing was carried out at both room temperature and 500°F with the strain range varying from 0.37% up to 1%. The resultant LCF curves are shown in Figure 16.

Between 2,000 and 10,000 cycles, data points taken at three temperatures are shown (R.T., 500°F, 1000°F). Within the scatter, there seems to be little difference in the cycles to failure at similar strain ranges. This suggests that the LCF life of the MAR-M247 GX, particularly in the revised heat treat condition, is relatively insensitive to test temperature over the range in temperatures from room temperature to 1000°F.

Compact Tension/Fatigue Crack Growth Rate

Fracture toughness testing using both the compact tension method and negative R ratio crack growth rate measurements using a K_B specimen were carried out in this task. One specimen was fracture toughness tested using the specimen configuration shown in Figure 17. Due to the limited amount of material available in a Titan rotor, the specimen thickness was not sufficient for a plane strain condition. The apparent fracture toughness, K_Q, was found to be 70.8 ksi-$in^{1/2}$, which compares with a value obtained with the aged only heat tr

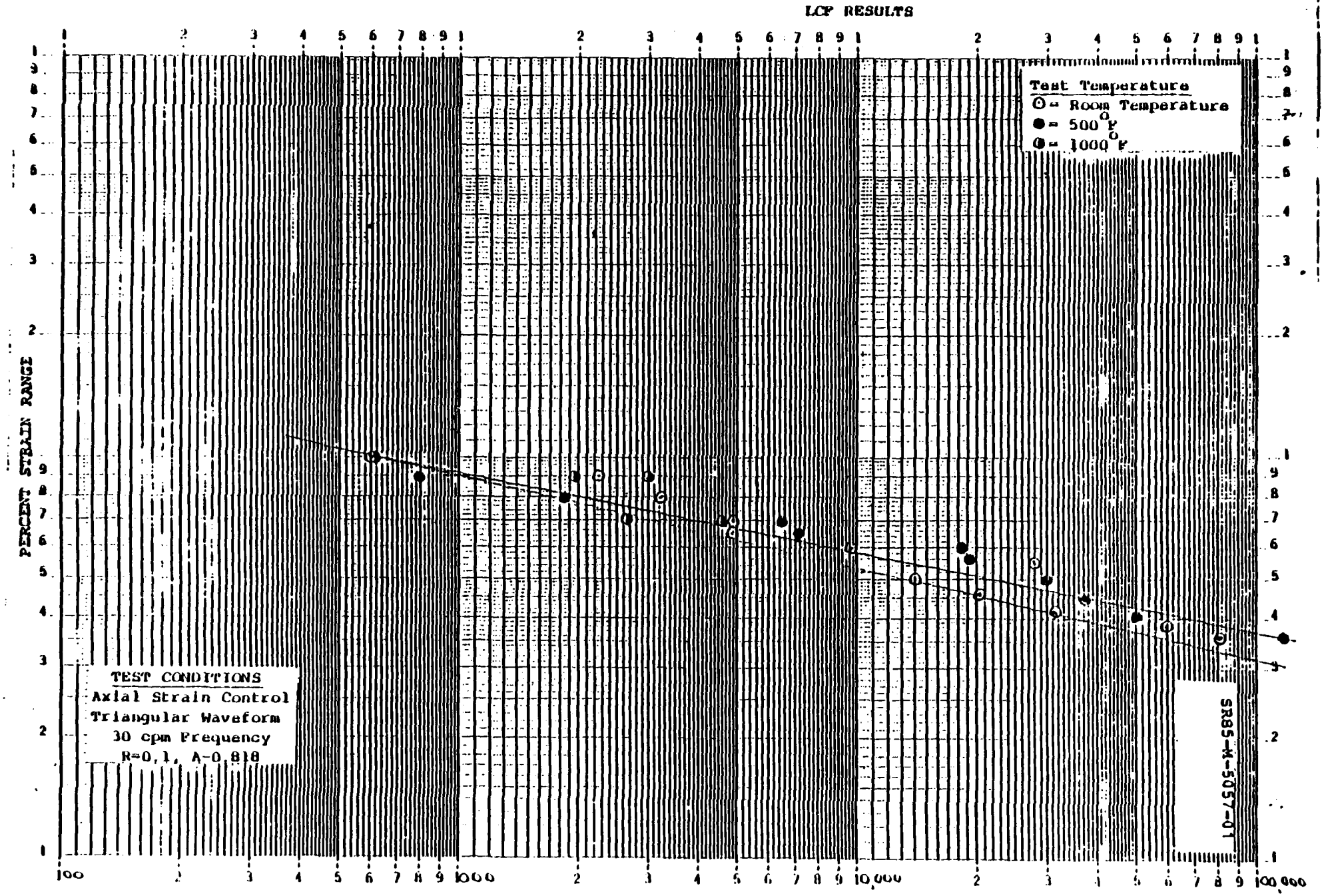

FIGURE 16. MAR-M247 LCF CURVES

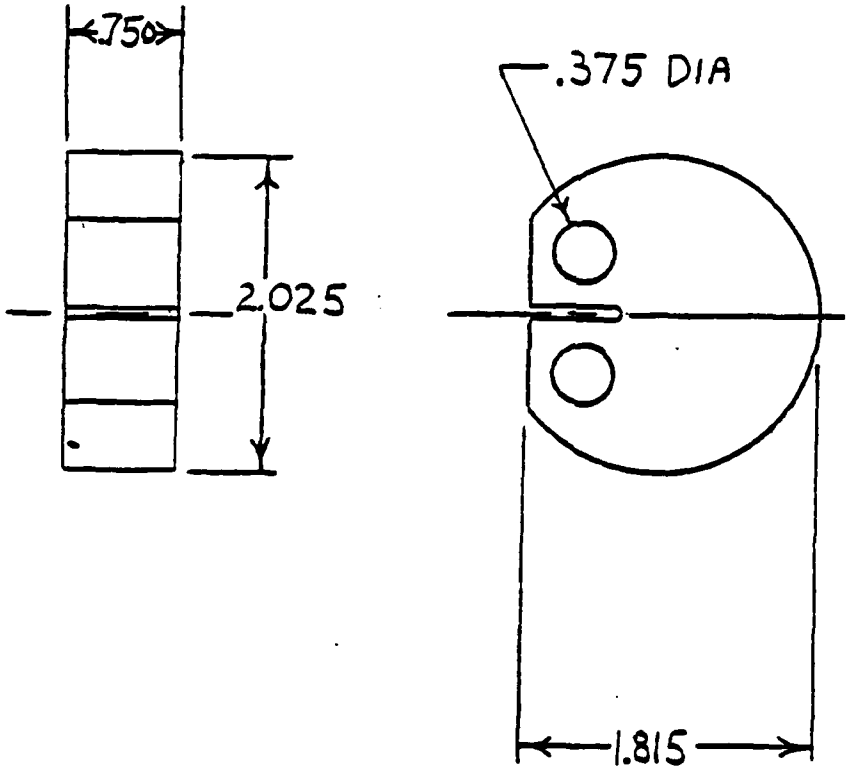

FIGURE 17. K_b COMPACT TENSION TEST SPECIMEN USED FOR FRACTURE TOUGHNESS TESTING.

A crack growth specimen configuration was selected so that negative R ratio crack growth measurements could be made. It was the intent of the task to establish whether or not the compressive part of the loading cycle influenced the crack growth rate. The specimen configuration used for this testing is the K_B specimen shown in Figure 18. The specimen configuration has a known crack tip geometry allowing accurate determination of the stress intensity and is capable of sustaining a compressive load. Testing was performed by Metcut Research Associates, Cincinnati, Ohio. Testing conformed to ASTM E647, Constant-Load-Amplitude Fatigue Crack Growth Rates Above 10^{-8} m/cycle and NASA TM-83200. Four tests were performed with the parameters shown in Table IX. The results are shown on the d(2c)/dN vs. ΔK plot, Figure 19. Testing was performed at 1100°F and at a frequency of 0.5 Hz.

Table IX. K_B Crack Growth Rate Test Parameter

S/N	R Ratio	Max. Stress	Min. Stress
3A-58	-0.3	120 ksi	-36 ksi
3A-66	-0.3	100 ksi	-30 ksi
3A-71	-0.5	100 ksi	-50 ksi
3A-73	0.10	100 ksi	10 ksi

The R ratios tested ranged from -0.5 to 0.1. Comparing the R = -0.5 run with the R = 0.1 run, it is quite evident that the compressive loading cannot be neglected. Specimens S/N 3A-75, 3A-71, and 3A-66 were all loaded to the same maximum stress of 100 ksi with various R ratios. The data clearly shows three separate curves on the d(2c)/dN vs. ΔK plot. specimens S/N 3A-66 and 3A-58 were both tested at R = 0.3, but at 100 and 120 ksi maximum stress, respectively. The data for S/N 3A-58 appear to generally lie between

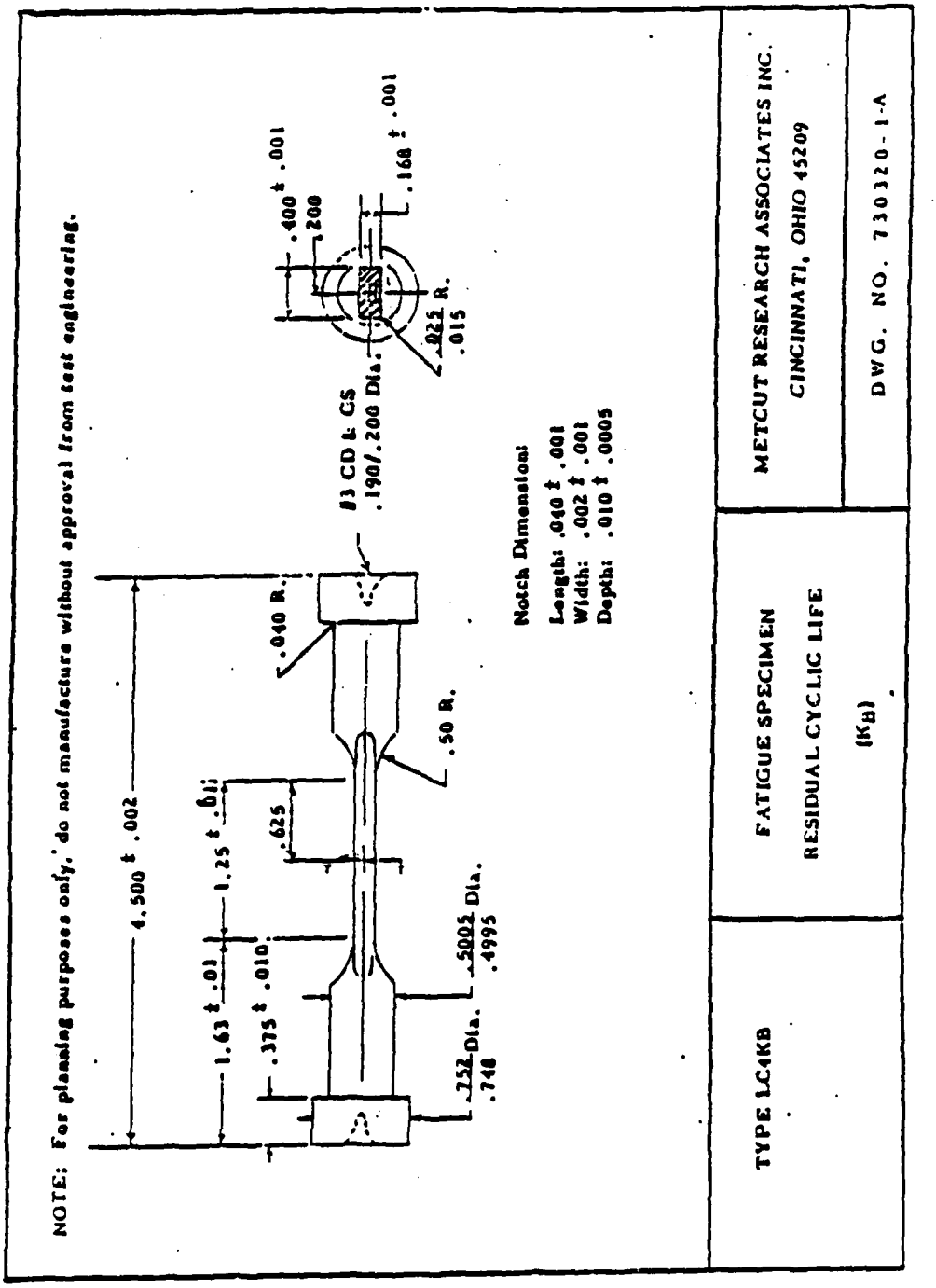

Figure 18. Fatigue Crack Growth Test Specimen Sketch

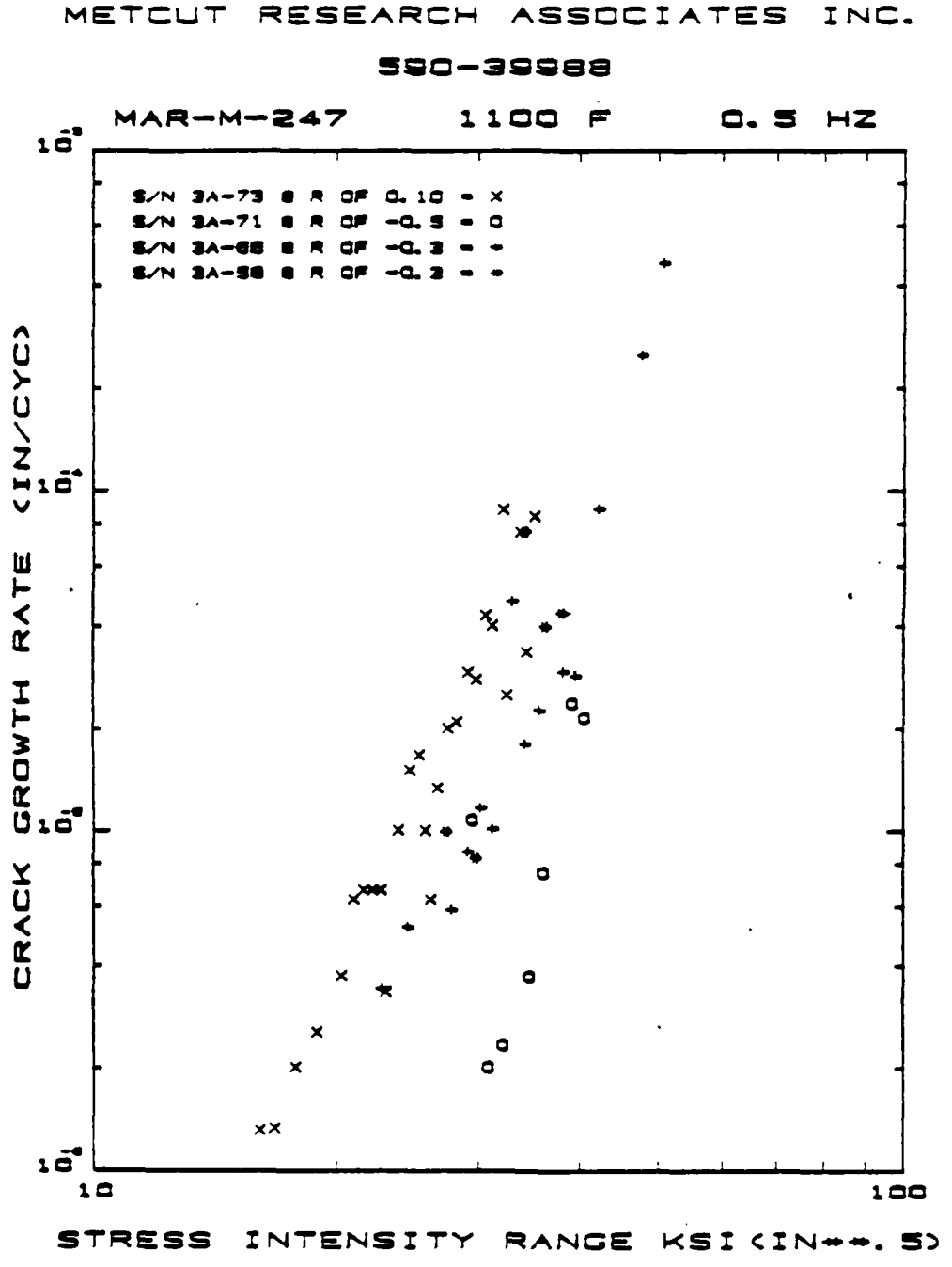

Figure 19. K_B Crack Growth Rate Plot

S/N 3A-71 and 3A-66 (see Figure 19). S/N 3A-58 had a total stress range of 156 ksi compared with 150 and 130 ksi for S/N 3A-71 and 3A-66, respectively. Even though S/N 3A-58 had a higher stress range than S/N 3A-71, it showed a lower crack growth rate. This may indicate an increased importance in the compressive part of the load cycle. Unfortunately, due to the high tensile loading on S/N 3A-58, only a few data points were taken before failure, making it difficult to draw valid conclusions.

II. IMPROVED BEARING AND LUBRICATION SYSTEM PROGRAM

2.0 INTRODUCTION

Sundstrand Turbomach has received Contract N00019-8-G-0603 from the United States Department of the Navy, Naval Air Systems Command, Washington, D.C., for the purpose of conducting a product improvement program for Turbomach T-62T auxiliary power units. The program consists of two areas of investigation:

1) Corrosion Resistant Turbine Wheel
2) Improved Bearing and Lubrication

Section II of this report covers the Improved Bearing and Lubrication System investigation and satisfies the final requirement of the program. This report represents the completion of the obligations as defined in the Statement of Work.

2.1 PROGRAM STATUS

The following table details the status of obligations defined in the Statement of Work.

II. Improved Bearing and Lubrication

Task	Status
Design Oil Jet Cartridge	Complete
Procure Parts	Complete
Assemble Test Engine	Complete
Conduct Flow Test	Complete
Prepare Final Report	Complete

2.2 BACKGROUND

A new oil jet cartridge was tested on the T-62T-40C APU with very favorable results. The new oil jet cartridge employed a system of seven oil jets which were thought to provide a more efficient distribution of lubricating oil. The successful application of the new cartridge on the T-62T-40C prompted an effort to employ the cartridge on the T-62T-11, T-62T-27, and T-62T-40-1 engines. It was thought that these engines would also benefit from the new lubrication system. However, initial tests indicated that the cartridge actually had a detrimental effect when used in these APUs. As a result, the program was discontinued to avoid unnecessary expenditures. A summary of the investigation follows.

2.3 CONCLUSION

The proposed oil jet cartridge failed to reduce bearing temperatures in any of the configurations tested. Consequently, a thorough investigation will be required to isolate and analyze the variables which influence the lubrication and bearing systems. The goal of the proposed work will be to do a detailed analysis of the bearing and lubrication systems on the Titan T-11, T-27, and T-40-1 auxiliary power units in order to define the area that is creating the heat/vibration. Current estimates indicate that the proposed analyses would require funding of $85,727. The projected cost and schedule to complete the proposed analyses are shown in Figures 20 and 21. (A detailed proposal can be provided if requested.) Actual and projected costs for work performed to date are shown in Figure 22.

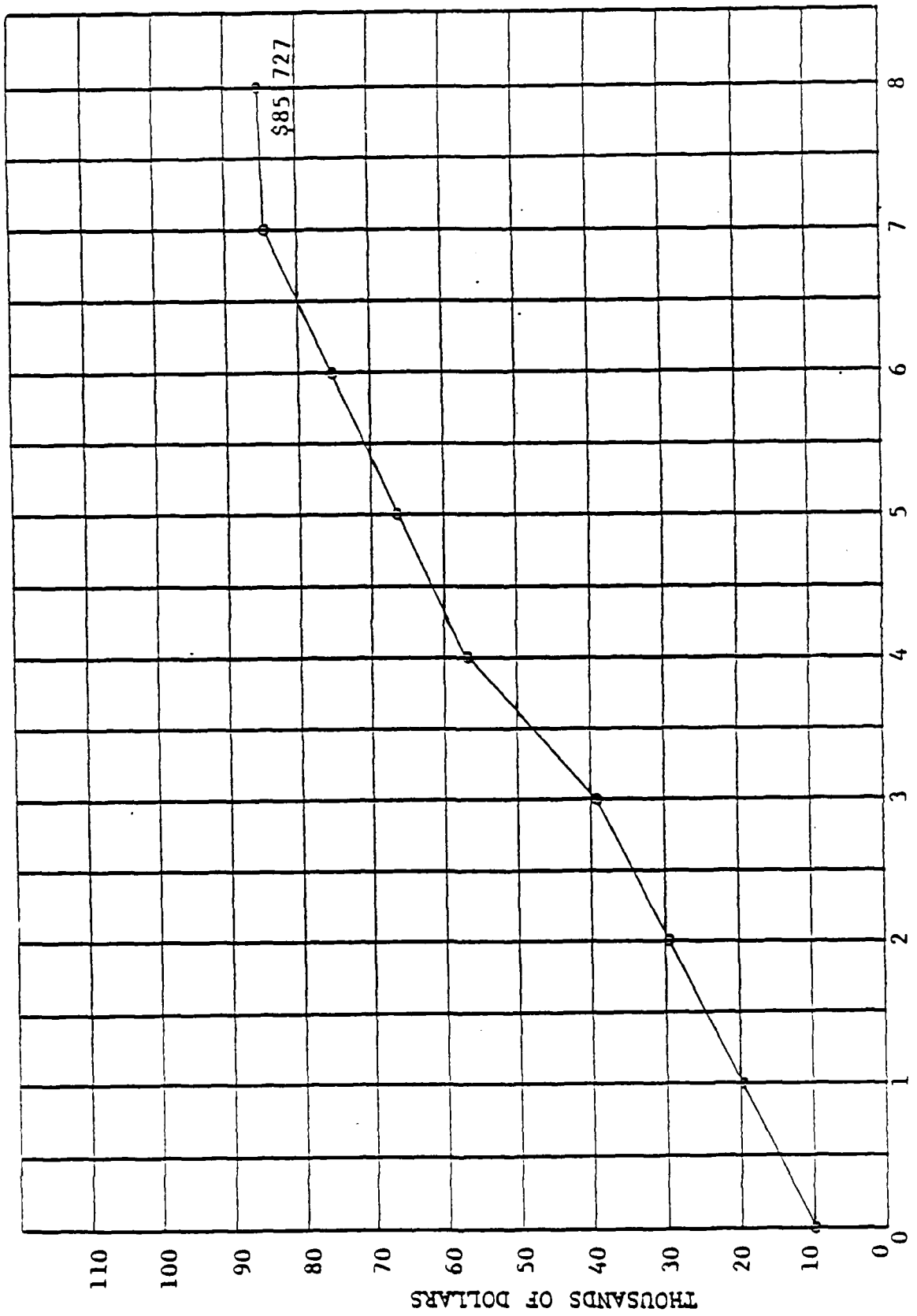

FIGURE 20. PROJECTED PERFORMANCE AND COST CURVE FOR PROPOSED LUBRICATION AND BEARING SYSTEM ANALYSIS.

IMPROVED BEARING AND LUBRICATION PROGRAM SCHEDULE

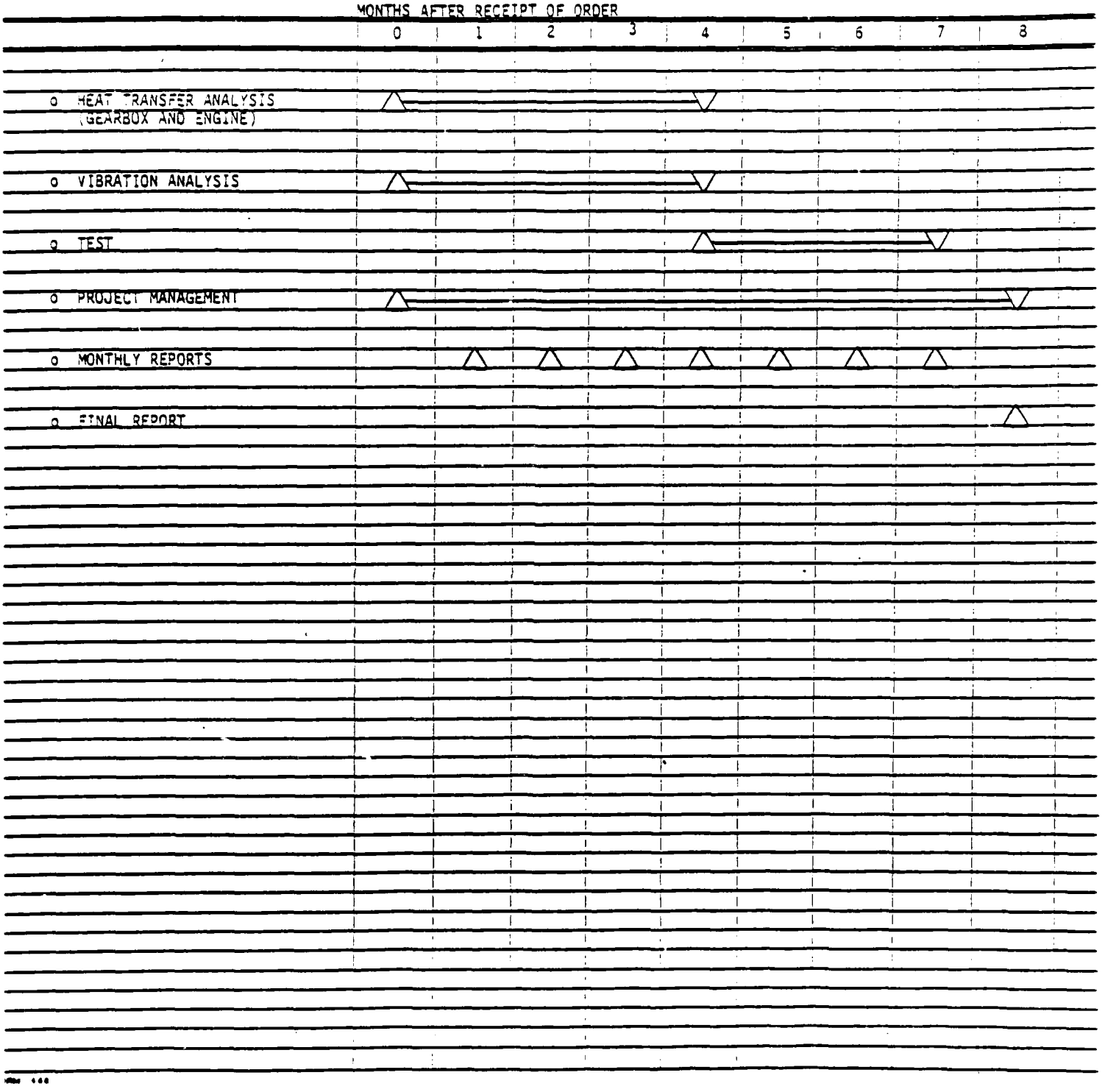

FIGURE 21. PROGRAM SCHEDULE FOR REVISED LUBRICATION AND BEARING SYSTEM ANALYSIS.

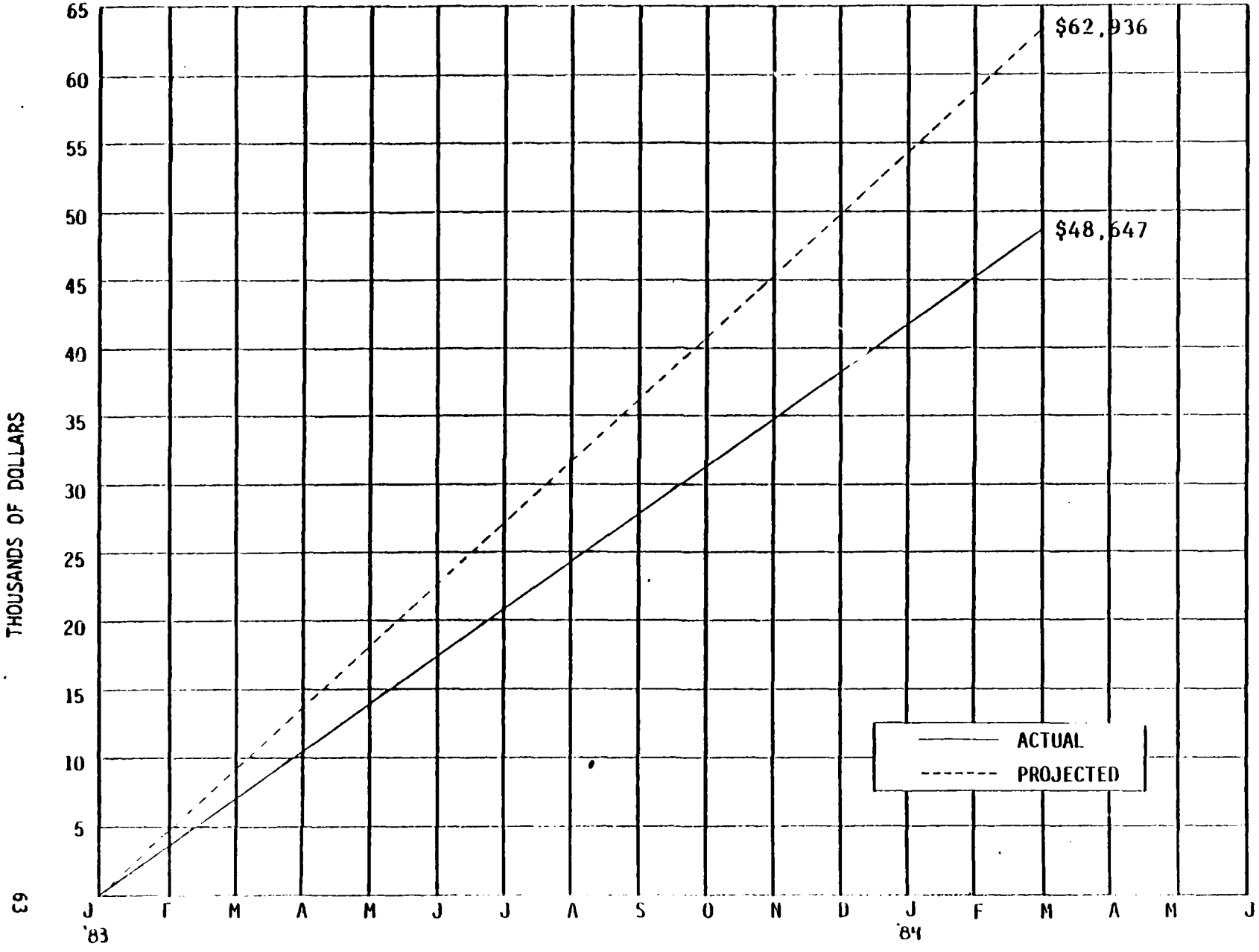

FIGURE 22. PERFORMANCE AND COST CURVE FOR WORK PERFORMED TO DATE

2.4 TECHNICAL DESCRIPTION

In order to improve the reliability of the bearing and lubrication systems in the T-62T-11, T-62T-27, and T-62T-40-1 auxiliary power units, a new oil jet cartridge was proposed to replace the existing oil jet ring. Figure 23 illustrates the basic components of the existing lubrication system. The oil pump, which is built into the gearbox, draws oil out of the gearbox sump and forces it through a ten-micron oil filter. From the filter, oil is forced into a passage to the pressure relief valve and the three oil jets located in the oil jet ring. (See Figure 24.) The oil jet ring is fitted inside the pinion gear shaft in the gear reduction assembly. The oil jet ring encircles the high speed input pinion and provides three jets of oil that are directed at the mesh points of the input pinion and planetary gears. The proposed modification would have substituted the existing oil jet ring with an oil jet cartridge which employed a system of seven oil jets. (See Figures 25 and 26.) The purpose of the new oil jet cartridge was to provide a more efficient distribution of lubricating oil to the pinion and planetary gears. This would improve the reliability of the bearing and lubrication system reducing bearing temperatures and increasing bearing life.

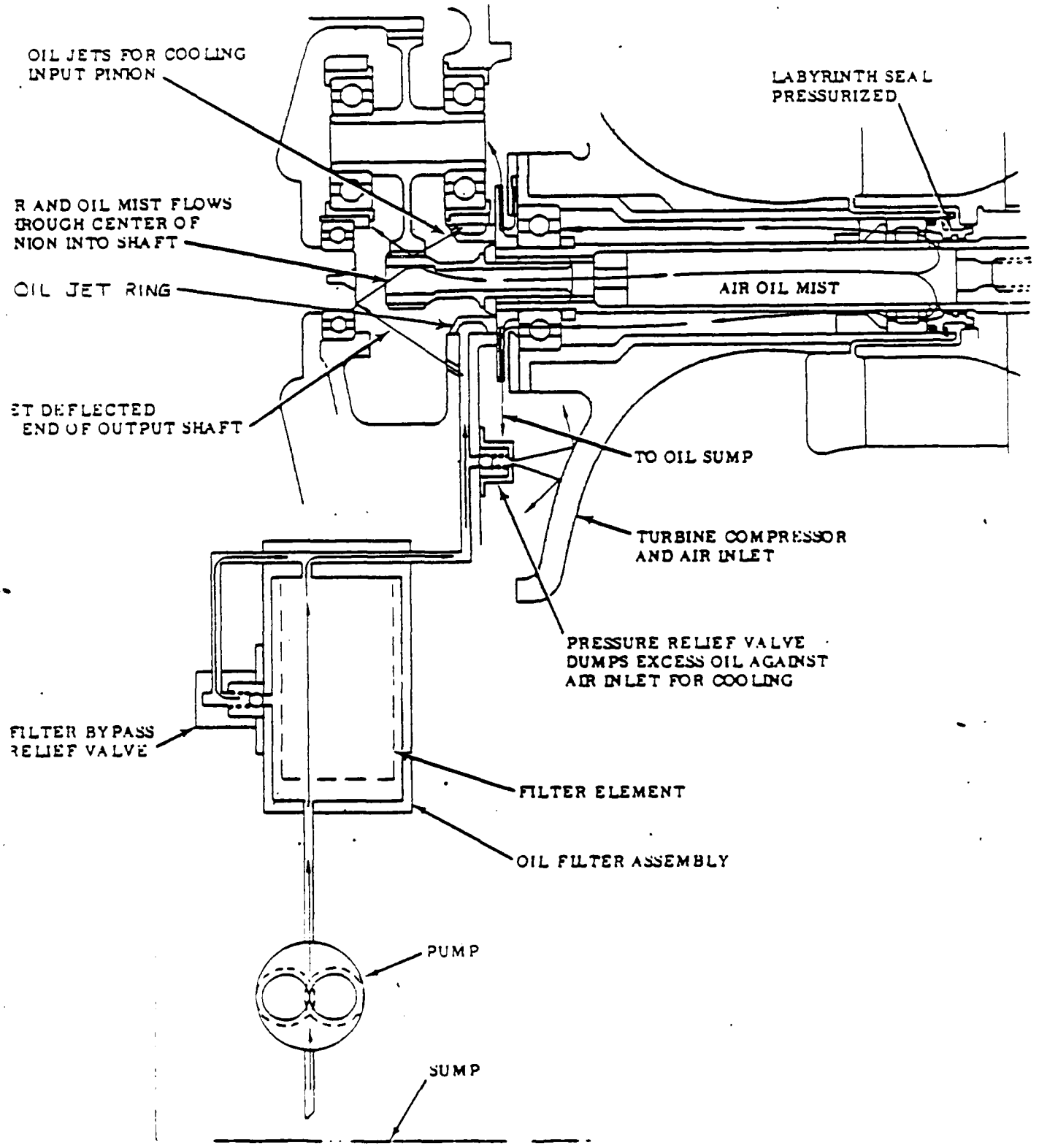

FIGURE 23. LUBRICATION SYSTEM SCHEMATIC.

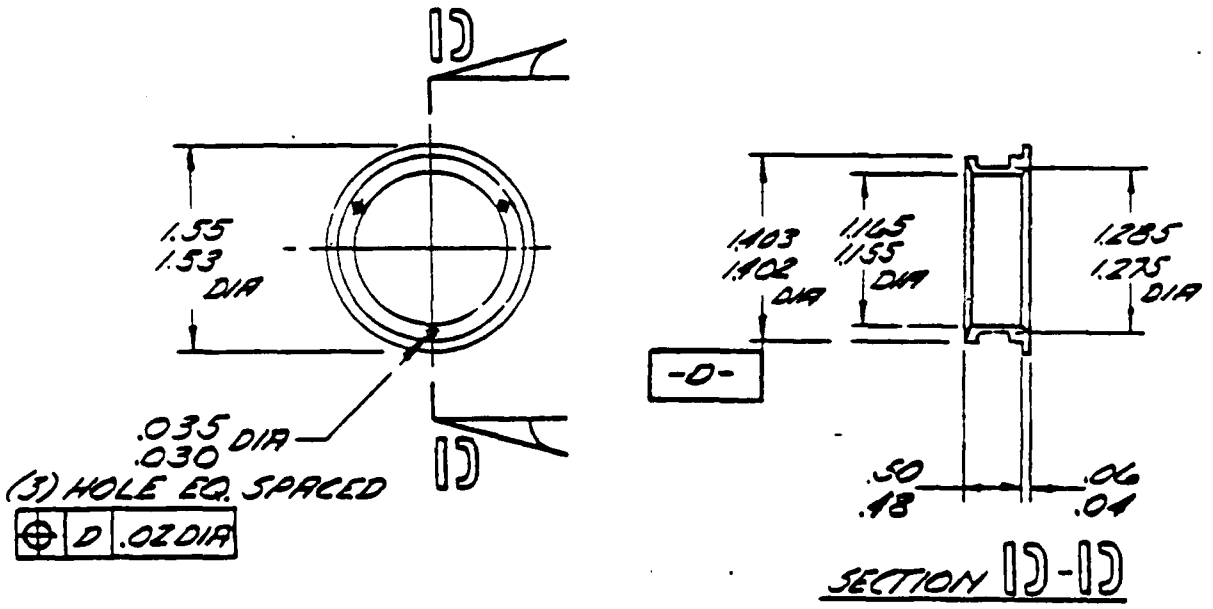

Figure 24. Oil Jet Ring Detail Drawing

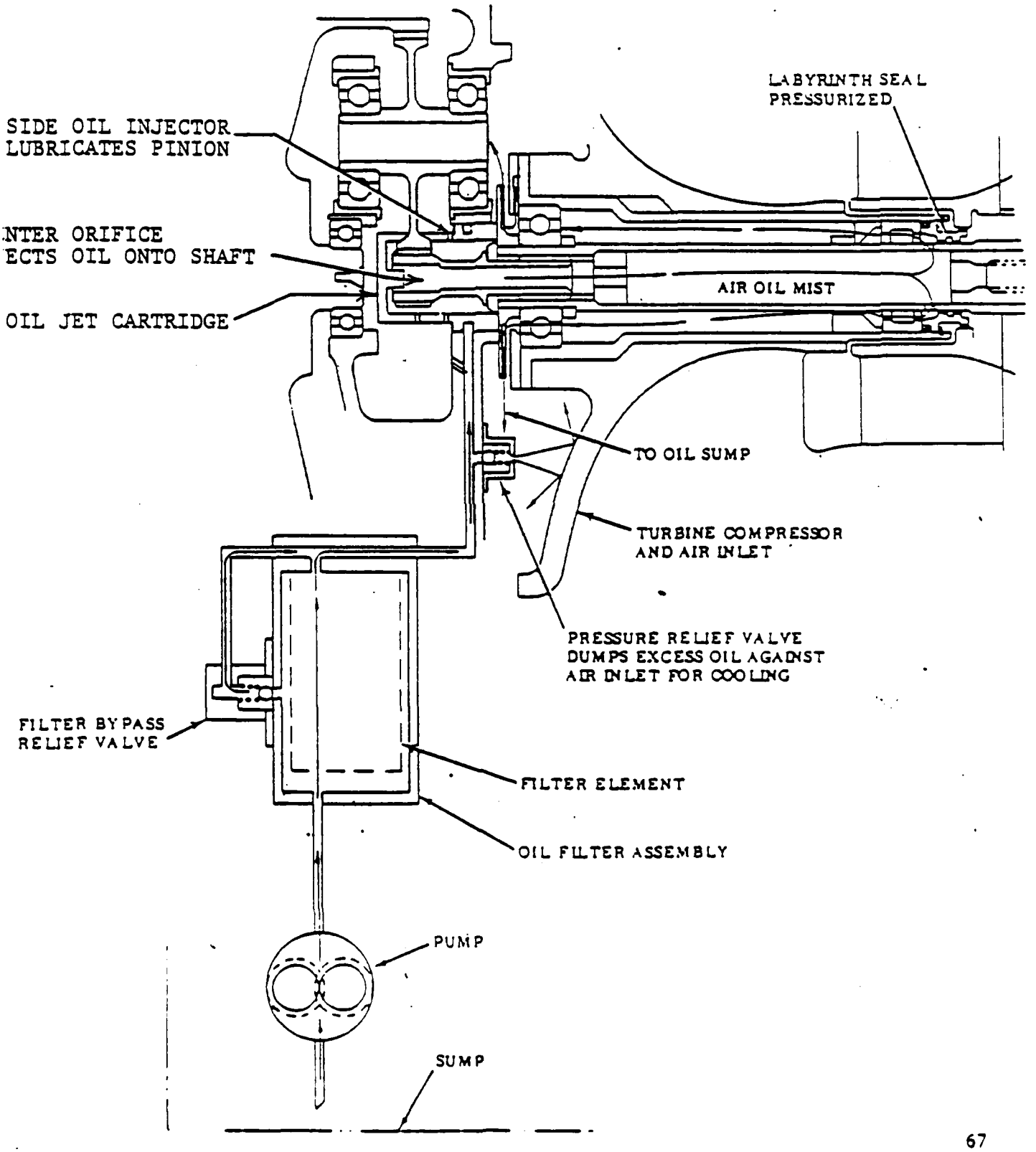

FIGURE 25. PROPOSED LUBRICATION SYSTEM SCHEMATIC.

DIMENSIONS IN INCHES

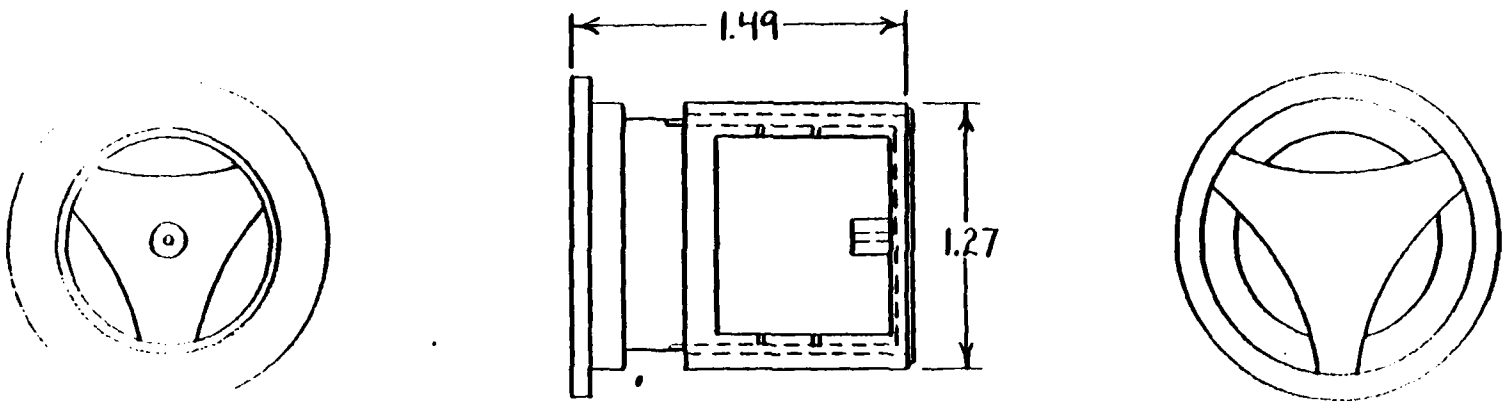

FIGURE 26. OIL JET CARTRIDGE DETAIL DRAWING

2.5 RESULTS

The performance of the oil jet cartridge was evaluated by running comparison tests between the standard oil jet ring and the oil jet cartridge. (See Appendix A.) Oil and bearing temperatures were recorded using several configurations of the oil jet cartridge and compared to equivalent temperature measurements using the standard oil jet ring. Initially, the cartridge employed a center hole jet diameter of 0.25 inch. The results of tests run in this configuration are shown in Table X. It was thought that the elevated temperatures recorded using the cartridge were a result of an overabundance of oil. Consequently, the center hole jet diameter was reduced to 0.020 inch and the test was repeated with similar results. This second test had to be shut down after only six minutes as the aft bearing temperature was nearing 300°F with no indication of stabilizing (see Table XI). Subsequent tests with minor cartridge configuration changes also produced unfavorable results.

Table X. Lube Oil and Bearing Temperature Comparison Between Oil Jet Ring and Oil Jet Cartridge at 1200°F EGT

	Test Start (+5 minutes)			Steady State (+15 minutes)		
	Oil Ring	Cartridge*	%Δ	Oil Ring	Cartridge*	%Δ
Lube oil °F	180	198	+10.0	203	228	+12.3
Fwd. bearing °F	239	250	+4.6	255	267	+4.7
Aft. bearing °F	240	270	+12.5	253	292	+15.4

*Center hole jet diameter = 0.025 inch

Table XI. Lube Oil and Bearing Temperature Comparison Between Oil Jet Ring and Oil Jet Cartridge*

	EGT = 800°F			EGT = 900°F		
	Oil Ring (+30 min)	Cartridge (+6 min.)	%Δ	Oil Ring (+30 min)	Cartridge (+6 min)	%Δ
Lube oil °F	235	193	-17.9	238	215	-9.7
Fwd. bearing °F	116	248	+113.8	115	261	+127.0
Aft. bearing °F	266	270	+1.5	268	290	+8.2

*Center hole jet diameter = 0.020 inch

APPENDIX A

T-62T-40-1 BEARING LUBRICATION TESTS

SOLAR TURBINES INCORPORATED

INTEROFFICE MEMO

TO: DISTRIBUTION

FROM: JESSE GARCIA

SUBJECT: T-62T-40-1 BEARING LUBRICATION TESTS

DATE: SEPTEMBER 9, 1982

The T-62T-40-1 carrier assembly currently includes an oil ring element, P/N 116194-4. An oil cartridge of new design, P/N 161777 has been tested with negative results. Table I below states the results of comparative tests between the standard oil ring and the newly designed oil cartridge. Refer to ERR-0254 for the test plan. The oil and bearing temperatures were recorded at 5 minutes after test start, and at steady state.

TABLE I
(°F)

1200 °F EGT

TEST DATE 6/25/82	EXISTING OIL RING		NEW OIL CARTRIDGE	
	TEST START (+5 Min)	STEADY STATE	TEST START (+5 Min)	STEADY STATE
Lube Oil Temp.	180	203	198	228
Fwd. Br. Temp.	239	255	250	267
Aft Br. Temp.	240	253	270	292

As a result of the above, it was recommended that the center hole jet diameter be reduced from .025" to .020" in the belief that an overabundance of oil was the source of higher bearing and oil temperatures. The modification was made and the oil cartridge was tested coincidently with the potential flow range improvement test (reference ERR-0265). Although the test procedure (referring to the latest test) was not identical to previously performed tests, it was concluded from the results that the oil injection lube system functioned in an unacceptable manner.

Temperatures with the oil cartridge installed, rose quickly upon start-up and reached higher temperatures in far less time than for the oil ring. The aft bearing temperature gave no indication of stabilizing and exhibited a maximum temperature of 296°F before shutdown. The flow range improvement test was completed with the cartridge replaced by the standard oil ring. Table II below lists a set of data point values for each of the two designs during the latest test.

TABLE II

TEST DATE 8/30 - 9/1	EXISTING OIL RING 30 MIN. RUNNING TIME					NEW OIL CARTRIDGE 6 MIN. RUNNING TIME		
Approx. EGT	640	700	800	900	1000	555	800	900
Lub. Oil T	223	230	235	238	240	156	193	215
Fwd. Br. T	112	114	116	115	115	231	248	261
Aft. Br. T	262	263	266	268	272	255	270	290

These latest test results suggest the newly designed oil cartridge may function as expected by instead enlarging the diameter of the center hole jet from its present .020" to .030".

Jesus Garcia

JG/ls

DISTRIBUTION

D. J. Martin
R. B. Fleming
R. G. Murison

END

4-87

DTIC